ChemCatChem

The European Society Journal for Catalysis

Chemistry Europe

European Chemical Societies Publishing

Supported by GECATS GERMAN CATALYSIS SOCIETY

Accepted Article

Title: Effect of support properties on selective butanediols production from erythritol using Ir/ReOx catalysts

Authors: Emanuel Martín Virgilio, Cristina L. Padró, and María Eugenia Sad

To be cited as: *ChemCatChem* 10.1002/cctc.202100797

Link to VoR: https://doi.org/10.1002/cctc.202100797

WILEY-VCH

FULL PAPER WILEY-VCH

Effect of support properties on selective butanediols production from erythritol using Ir/ReO_x catalysts

Emanuel M. Virgilio, Cristina L. Padró, María E. Sad*[a]

[a] Emanuel M. Virgilio, Prof. Cristina L. Padró, Prof. María E. Sad
Catalysis Science and Engineering Research Group (GICIC), INCAPE,
UNL-CONICET, Predio CCT Conicet Santa Fe, Colectora RN 168 km 0, Paraje El Pozo, (3000) Santa Fe, Argentina
E-mail: evirgilio@fiq.unl.edu.ar, cpadro@fiq.unl.edu.ar, mesad@fiq.unl.edu.ar

Supporting information for this article is given via a link at the end of the document.

Abstract: This study reports the selective obtaining of butanediols (BDO), widely used in the polymer and synthetic rubber industry, by C-O hydrogenolysis of erythritol. The effect of the support on catalytic activity and selectivity to BDO was exhaustively studied using Ir/ReO_x catalysts supported on SiO_2, Al_2O_3, activated carbon, CeO_2, TiO_2 and ZrO_2. The catalysts were thoroughly characterized and it was found that the physicochemical, redox and acidic properties of the supports notably influenced the metal dispersion, reducibility of the species and particle sizes. The most active and selective catalyst was Ir/ReO_x/TiO_2 (maximum BDO yield of 53%), favoring C-O hydrogenolysis and minimizing C-C scissions and dehydration reactions. This superior performance was attributed to the formation of small clusters with an intimate contact between Ir and partially oxidized Re species (mainly Re^{+IV}) that favors the appropriate adsorption of erythritol on ReO_2 and the further interaction with H_2 adsorbed on Ir^0 to render BDO.

Introduction

The synthesis of chemical intermediaries and fuels, traditionally obtained from non-renewable sources of fossil origin, is being replaced by new processes involving biomass, which has several advantages over fossil fuels, such as: limiting the impact of dioxide of carbon on global warming and have a cycle of regeneration in the order of years and not millions of years. Therefore, new routes starting from biomass-derivate reactants are absolutely essential in order to produce useful chemicals and fuels[1–3]. However, usually biomass-related materials present higher oxygen content (O/C ratio) than most of the commodity and valuable chemicals, thus the development of catalytic routes to deoxygenation of such substrates is greatly desired. Among the deoxygenation methods, selective hydrogenolysis of C-O bond is an important strategy to remove the hydroxyl groups of oxygenated biomass-derived molecules.

Erythritol (ERY) is a polyol of chemical formula $C_4H_{10}O_4$ that is commercially produced through fermentation[4–7] of glucose and sucrose from chemically and enzymatically hydrolyzed wheat and corn starches[8,9]; it is used as low-calorie sweetener and as a functional sugar substitute for people with diabetes and obesity[4]. Due to the high yield and productivity in the industrial scale of production, erythritol serves as starting material for the production of other sugars and because of its high functionality it is suitable of being transformed into valuable intermediates. [10]

C-O hydrogenolysis of ERY allows to obtain butanediols (BDO), which are valuable chemicals used in the industry of synthetic rubber and polymers as intermediates in the production of tetrahydrofuran, polytetramethylene-ethylene glycol, polybutylene terephthalate and polyurethane, among others[11]. C4-diols can also be considered as versatile chemical building blocks, useful for coating applications[12] or for producing butadiene[13,14]. There are four butanediols: 1,4-butanediol (1,4BDO), 1,3-butanediol (1,3BDO), 1,2-butanediol (1,2BDO) and 2,3-butanediol (2,3BDO). 1,4BDO is widely used in industry, particularly in the production of polyurethanes and polybutylene terephthalate (PBT) as well as in the production of ɣ-butyrolactone (GBL) and tetrahydrofuran (THF)[15]. Currently, 1,4BDO is mainly produced through the hydrogenation of maleic anhydride obtained from butane oxidation[16]. 1,3BDO is used in the food flavorings industry as organic solvent and is a raw material for production of polyurethane and polyester resins. 1,3BDO is produced via aldol condensation of acetaldehyde[17] which is produced by the Wacker oxidation of ethylene. 1,2BDO is generated as a by-product during the fabrication of 1,4BDO and is a precursor for the production of low viscous polyester and plasticizers[18]. 2,3BDO is used as a raw material for printing inks, perfumes, pharmaceuticals and fumigants and it is obtained from the microbial fermentation of monosaccharides[11].

Polyol hydrogenolysis has been widely studied, particularly using glycerol as reactant in aqueous solution to produce 1,2-propanediol[19] and 1,3-propanediol[20–22]. However, many times the rupture of C-C bonds, together with C-O cleavages, is also desired in order to produce compounds with lower number of C atoms as for example ethylene glycol. Typically, metal/support catalysts are used to catalyze hydrogenolysis reactions being the noble metal the most active and frequently used catalysts. Silica-supported Pt, Ru, Rh, and Ir catalysts were investigated for the hydrogenolysis of glycerol[7,23–25]. Ruthenium is well known to be active in the hydrogenolysis of polyols such as glycerol[23,26,27], xylitol and sorbitol[28,29] but unfortunately, could promote excessive C–C cleavage[23]. Ir, Rh and Pt are also recognized as a catalyst for glycerol hydrogenolysis[30–34] but it was reported that Pt is typically less active than Ru or Ir. The combination of an oxophilic promoter (Re, Mo or W) with the highly reducible noble metal (Ru, Ir, Rh or Pt) improved the selective C-O bond hydrogenolysis of polyols and even, cyclic ethers such as tetrahydrofurfuryl alcohol[35–39] avoiding the C-C cleavage.

Despite the rather comprehensive study of the hydrogenolysis of other polyols, such as glycerol, there are few papers that use erythritol as raw material. The first study about hydrogenolysis of ERY was carried out by Montassier et al.[26] over Ru/C catalysts who reported a fast epimerization to ERY isomer, threitol and the obtaining of a complex mixture of products at 513 K and 40 bar of H_2 whereas the poisoning with sulphur, produced an

increment in the initial selectivity towards butanetriols (BTO) + BDO with 1,2BDO as the main isomer followed by 2,3BDO; however, no yield or conversion values were reported. Additionally, the use of noble metals such as Rh or Ir (3.5-4%) combined with a promoter like Re, W or Mo (4%) has been studied in the conversion of an aqueous solution of ERY. Yields of BDO and BTO of 29.6 and 23.2% respectively, have been reached using 3.7% Rh/3.5% ReO_x/ZrO_2 at 473 K and 120 bar H_2[39] whereas 25% of BDO yield was recently achieved on 4% $Ir/ReO_x/TiO_2$ (rutile) at 373 K and 80 bar H_2[40]. The maximum yield towards BDO reported to date was 34.7% (24.4% 1,4BDO, 8.9% 1,3BDO, 0.7% 2,3BDO and 1,2BDO) obtained after 24 h of reaction using $Ir/ReO_x/SiO_2$ at 373 K and 80 bar H_2[41]. These results show that the hydrogenolysis of erythritol requires high temperature, H_2 pressure and concentration of metal in the catalyst, and a prolonged reaction time. Furthermore, these reports and previous studies using glycerol, suggest the convenience to use a multifunctional catalyst that includes metallic sites (Ir, Rh, Pt, Pd, Ru) and partially oxidized species of another metal such as Re, W or Mo. It is important to remark that SiO_2, despite its low hydrothermal stability[42], has been the solid mostly used as support. According to our best knowledge, there are no studies evaluating the role of the support during erythritol hydrogenolysis to yield butanediols. However, some studies on sorbitol hydrogenolysis using Ru supported on Al_2O_3, SiO_2, TiO_2 and ZrO_2[28] showed that the support has an effect on the physicochemical properties of the supported Ru particles and, consequently, in its catalytic activity. The purpose of this work is to evaluate the effect of the support on catalytic activity and selectivity towards the desired products (BDO) of catalysts based on Ir (~2%) and Re (~2%) supported on solids of different nature (SiO_2, Al_2O_3, ZrO_2, CeO_2, activated carbon and TiO_2).

Results and Discussion

Catalysts characterization

Structural and acid characterization

The physicochemical properties of the prepared catalysts (chemical composition determined by ICP and BET surface area) are presented in Table 1. The Ir and Re loadings ranged between 1.6-2.4 wt.% and 1.4-2.8 wt.%, respectively. The nominal Ir/Re molar ratio was 1 for the six catalysts; however, the actual Ir/Re ratio on Ir/ReO_x supported on Al_2O_3, AC, CeO_2 and TiO_2 was 0.70-0.83 whereas this ratio was about 1.3 for $Ir/ReO_x/SiO_2$ and $Ir/ReO_x/ZrO_2$. Nevertheless, it was previously reported for several polyols [41,43,44] that the Ir/Re molar ratio only modified the catalyst activity not noticing a substantial influence on product selectivities. The sequential impregnations and subsequent thermal treatments of the supports did not cause significantly change in the BET surface as can be noticed in Table 1. Ir/ReO_x/AC displayed the highest surface area in good agreement with results usually informed for this type of microporous material[45], $Ir/ReO_x/SiO_2$ and $Ir/ReO_x/Al_2O_3$ presented surface areas of 269 and 218 m^2/g whereas the S_{BET} for the rest of the catalysts were lower than 85 m^2/g. DRX spectra of Ir/ReO_x/support catalysts shown in Figure 1 indicate that no other phase different from the corresponding to the support was detected. Indeed, neither peaks around 2θ = 40.5º and 2θ = 28.0º assigned at Ir metal and a IrO_2 phase respectively nor diffraction peaks attributed to ReO_x or Re^0 (2θ = 34.9º for Re^0, 2θ = 24.3º for ReO_2, 2θ = 29.1º for ReO_3 and 2θ = 24.6º for Re_2O_7)[43] were detected by DRX.

Table 1. Physicochemical characterization

Catalyst	wt% Ir	wt% Re	Ir/Re molar	S_{BET}[a] (m^2/g)	TPD NH_3 (μmol/g)
$Ir/ReO_x/SiO_2$	1.87	1.44	1.26	269 (269)	32.6
$Ir/ReO_x/Al_2O_3$	1.70	2.10	0.78	218 (220)	353.1
Ir/ReO_x/AC	1.88	2.60	0.70	747 (861)	252.1
$Ir/ReO_x/CeO_2$	1.60	1.96	0.79	41 (45)	116.6
$Ir/ReO_x/TiO_2$	2.36	2.77	0.83	44 (50)	85.0
$Ir/ReO_x/ZrO_2$	2.23	1.67	1.29	82 (93)	84.9

[a] Support surface area in parentheses.

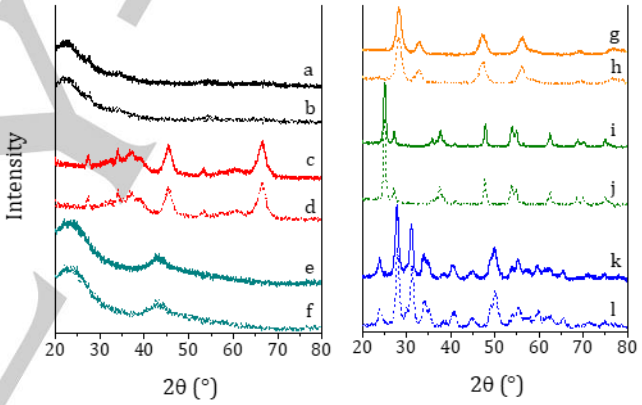

Figure 1. Sample characterization by X-ray diffraction: XRD diffractograms of bimetallic catalysts (full lines) and supports (dotted lines). a) $Ir/ReO_x/SiO_2$, b) SiO_2, c) $Ir/ReO_x/Al_2O_3$, d) Al_2O_3, e) Ir/ReO_x/AC, f) AC, g) $Ir/ReO_x/CeO_2$, h) CeO_2, i) $Ir/ReO_x/TiO_2$, j) TiO_2, k) $Ir/ReO_x/ZrO_2$, l) ZrO_2.

The acid sites density was calculated by integration of NH_3 TPD profile displayed in Figure S1, Supporting Information and the μmol NH_3/g catalyst are listed in Table 1. $Ir/ReO_x/Al_2O_3$ exhibited the highest concentration of acid sites followed by Ir/ReO_x/AC; in addition, this last catalyst presented the strongest acid sites according to the high temperature of the ammonia desorption peak (Figure S1, Supporting Information). $Ir/ReO_x/TiO_2$ and $Ir/ReO_x/ZrO_2$ displayed similar density of acid sites (85 μmol/g) whereas $Ir/ReO_x/SiO_2$ was the least acidic catalysts as expected. It was previously demonstrated that the Re species, with Re not totally reduced, could generate Lewis acid sites on the catalyst surface[46]. Thus, the contribution of Re species to the acidity of the catalysts, studied by comparing the amount of acid sites on the bimetallic samples and the bare supports, is displayed in Table S1 and Figure S2 of Supporting Information. The acidity attributed to the metal addition on the support ranged between 25 and 42 μmol/g. In the case of $Ir/ReO_x/SiO_2$, the metal addition was responsible of the almost the total amount of acid sites in

the catalysts whereas the acidity of alumina clearly predominated in the case of $Ir/ReO_x/Al_2O_3$. Regarding $Ir/ReO_x/TiO_2$, a similar amount of acid sites came from the support and the addition of metal Re species.

Metallic phase characterization

Metallic phase of catalysts was studied by temperature programmed reduction (TPR), CO chemisorption, TEM and XPS. Figure 2 (A-F) shows the TPR profiles for monometallic Ir/support and ReO_x/support as well as for bimetallic Ir/ReO_x/support catalysts. The reduction profiles of Ir/support catalysts evidenced two reduction peaks attributable to the progressive reduction of different oxidized Ir species to Ir^0 whose shape and position seems to be affected by the Ir interaction with the support. The first peak, probably due to Ir^{+IV} to Ir^{+III} reduction, arise at low temperatures (398-463 K) and the second peak, accounting for the further reduction to metallic state, at about 513-553 K[47]. The reduction of Ir species was completed at 573 K since a H_2/Ir ratio closed to the stoichiometric ratio (H_2/Ir = 2) was calculated except in the case of Ir/CeO_2 (Table 2). The H_2 consumption for Ir/CeO_2 greatly exceeded the theoretical required for the sole reduction of the Ir oxides probable due to some ceria reduction[48,49]. Actually, bare ceria is reduced between 600-900 K (Figure S.2 Supporting Information) but the presence of a metal able to adsorb and dissociate H_2, as Ir, can strongly shift to lower temperature the reduction of the ceria in the vicinity of Ir. Likewise, the TPR profile of Ir/AC displayed a high H_2 consumption at temperatures higher than 673 K that can be ascribed to reduction of the support[45]; also some reduction of TiO_2 could be evidenced at temperatures higher than 873 K on Ir/TiO_2[50].

The reduction profiles of ReO_x/support catalysts presented in Figure 2 revealed that the reducibility of ReO_x species is greatly affected by the support. Thus, one or two peaks were detected in the range of 533-723 K similarly to other TPR profiles reported in literature[51]. The reduction of supported Re oxides has been interpreted as an autocatalytic process[52] where the reduction of more reactive ReO_x surface species (first H_2 consumption peak) induces the reduction of the less reactive ReO_x species (second peak). An *in situ* investigation using Raman, FTIR and TPR experiments for ReO_x (1-6 wt.% Re) on Al_2O_3, SiO_2, ZrO_2 and TiO_2 revealed that the rhenium oxide possesses a similar structure on all supports studied, with three Re=O and one Re-O-support bonds[51]. The H_2/Re ratio estimated from TPR profiles ranged 2.9-3.2 (Table 2), lower than the stoichiometric value (3.5) considering the full reduction of Re^{+VII} to Re^0 except for ReO_x/CeO_2 since the partial reduction of the support could probably provoke an increase of this H_2/Re ratio above the theoretical. This intermediate oxidation state for ReO_x species was previously reported in literature for similar bimetallic catalysts[53].

TPR profiles of Ir/ReO_x/support displayed at least two reduction peaks (Figure 2); the first peak presented a maximum at temperatures lower than 483 K whereas the high temperature peak was observed at 478-566 K. Activated carbon and, in less extent, reducible supports such as TiO_2, also showed a peak assigned to the partial support reduction; as previously discussed, CeO_2 was also reduced in some extent, although its reduction peak in $Ir/ReO_x/CeO_2$ profile was overlapped to the Ir and ReO_x reduction.

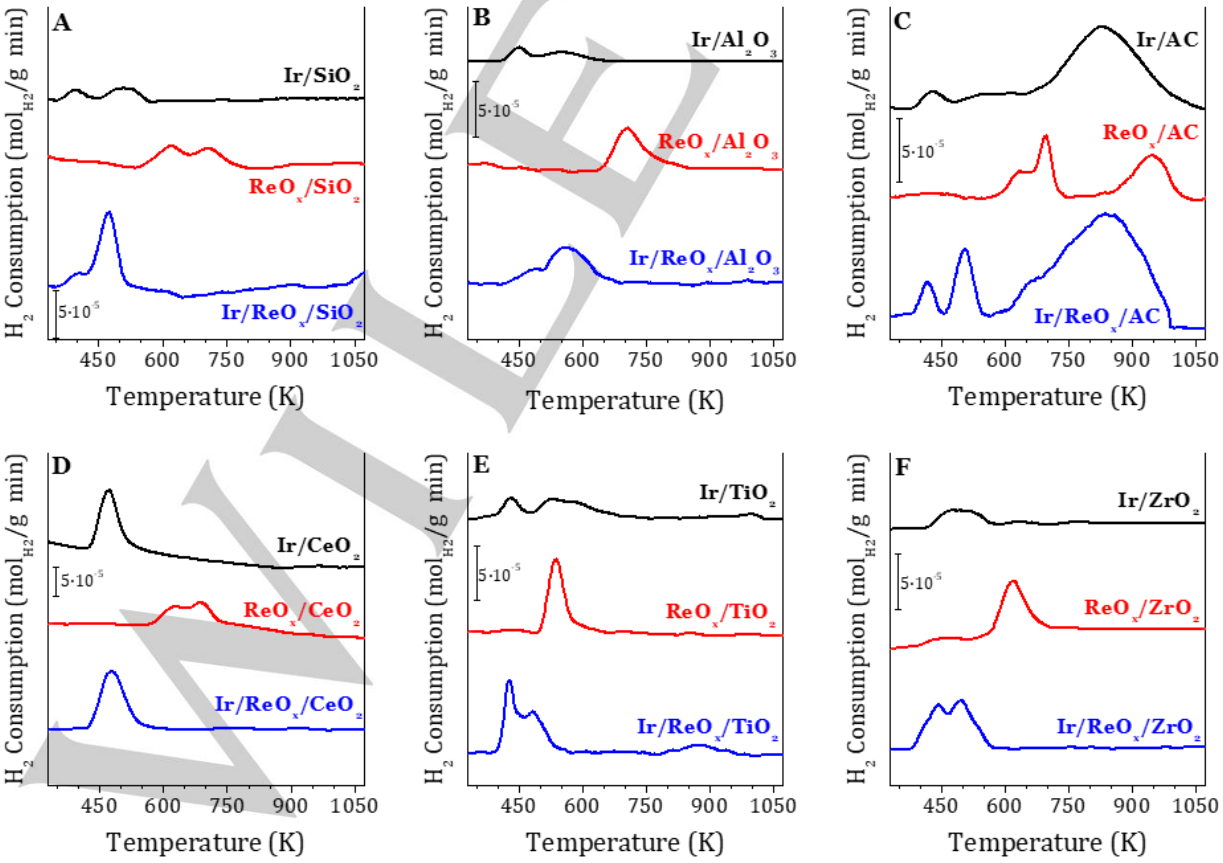

Figure 2. TPR profiles for catalysts supported on (A) SiO_2, (B) Al_2O_3, (C) AC, (D) CeO_2, (E) TiO_2 and (F) ZrO_2.

Table 2. Catalysts characterization by TPR.

Catalyst	H_2/Ir	Catalyst	H_2/Re	Catalyst	H_2/Total Metal	Peak 1 (H_2/Ir)	Peak 2 (H_2/Re)
Ir/SiO_2	1.8	ReO_x/SiO_2	3.0	Ir/ReO_x/SiO_2	2.62	1.32	4.25
Ir/Al_2O_3	1.7	ReO_x/Al_2O_3	3.2	Ir/ReO_x/Al_2O_3	2.20	1.19	5.15
Ir/AC	1.8	ReO_x/AC	2.9	Ir/ReO_x/AC	2.99	1.99	3.68
Ir/CeO_2	7.2	ReO_x/CeO_2	3.9	Ir/ReO_x/CeO_2	3.82	4.85	3.01
Ir/TiO_2	2.3	ReO_x/TiO_2	2.9	Ir/ReO_x/TiO_2	2.67	1.17	4.18
Ir/ZrO_2	1.8	ReO_x/ZrO_2	2.9	Ir/ReO_x/ZrO_2	2.28	1.30	3.55

Since the H_2 consumption of the first peak was lower than the theoretical total reduction of Ir (except for ceria) and the second peak was greater than the total reduction of rhenium (Table 2), the first reduction peak would be attributed to the partial reduction of Ir^{+IV} and probably, some ReO_x species easily reducible due to close contact with Ir particles, whereas the second peak assigned to ReO_x species reduction could also include the reduction of some Ir. In fact, the proximity of the peaks attributed to Ir and ReO_x reduction that can be measured as the difference of their maximum (ΔT_{TPR}), would evidence the interaction between the two metals. The low surface area of CeO_2, TiO_2 and ZrO_2, would facilitate the intimate contact between Ir and ReO_x particles evidenced by a low difference in the maximum of the peaks ($\Delta T_{TPR} \leq 60$ K) whereas a $\Delta T_{TPR} \approx 100$ K for Ir/ReO_x/AC suggests less interaction between both metals. In addition, the shoulder at about 673 K on Ir/ReO_x/AC, which is coincident to the second peak in ReO_x/AC, would indicate the existence of some segregated ReO_x clusters. Overall, TPR profiles denoted the existence of different interactions between both the support and metals oxides and between Ir and ReO_x. Finally, the temperature of the first reduction peak was selected as the optimal temperature to treat the catalyst before reaction in order to reduce iridium to Ir^0 while Re remains partially oxidized (Ir/ReO_x/SiO_2: 403 K, Ir/ReO_x/Al_2O_3: 483 K, Ir/ReO_x/AC: 423 K Ir/ReO_x/CeO_2: 468 K, Ir/ReO_x/TiO_2: 418 K and Ir/ReO_x/ZrO_2: 443 K).

Table 3. CO chemisorption results and particle size.

Catalyst	Dispersion (D_{CO}, %)	Particle size ($d_{P\ CO}$, nm)	Particle size ($d_{P\ TEM}$, nm)
Ir/ReO_x/SiO_2	14	7.8	3.1
Ir/ReO_x/Al_2O_3	40	2.7	3.2
Ir/ReO_x/AC	50	2.1	1.7
Ir/ReO_x/CeO_2	76	1.4	1.2
Ir/ReO_x/TiO_2	56	1.9	1.6
Ir/ReO_x/ZrO_2	18	6.0	4.0

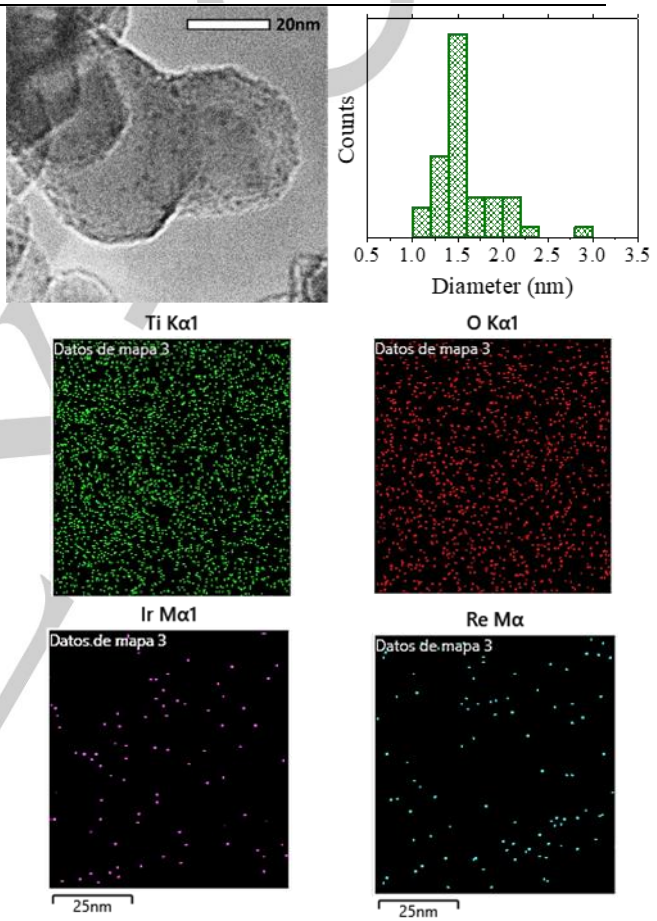

Figure 3. Representative TEM image, size distribution and EDS mapping associated with Ir/ReO_x/TiO_2.

Metal dispersion (D_{CO}) and particle size were estimated from CO chemisorption measurements and reported in Table 3. Ir/ReO_x/TiO_2 and Ir/ReO_x/CeO_2 presented the highest Ir dispersion (56 and 76 %) and accordingly, the smallest particle diameter (1.9 and 1.4 nm). Small particles sizes were also calculated on Ir/ReO_x supported on AC and Al_2O_3 (2.1-2.7 nm) corresponding to a dispersion of about 40-50%, while Ir/ReO_x/SiO_2 and Ir/ReO_x/ZrO_2 displayed the lowest Ir dispersion (14 and 18 % respectively) and their particle sizes from CO chemisorption were higher than 5 nm. Transmission electron microscopy (TEM) images of Ir/ReO_x/support catalysts were acquired and particle diameters were also estimated and included in Table 3. Figure 3 shows the high-resolution image,

the size histogram for Ir/ReO_x/TiO_2; the mean particle size was 1.6 nm in accordance to the value estimated from CO chemisorption. Similar particle sizes determined by TEM were reported by other authors on Rh/ReO_x/TiO_2[39,54,55] and Ir/ReO_x/rutile[40]; it was also informed[39] that Rh/ReO_x particles on ZrO_2 support were larger than on TiO_2 similarly to results in Table 3 for Ir-based catalysts. Both the particle size from CO chemisorption and the estimated from TEM were similar for all catalysts except for Ir/ReO_x/SiO_2 ($d_{p\,TEM}$ = 3.1 nm, less than half the $d_{p\,CO}$). This discrepancy can be attributed to a partial coverage of Ir metal particles with ReO_x clusters becoming part of Ir inaccessible to CO. A similar proposal has been also enunciated by Amada et al.[56] who had fully characterized Ir/ReO_x/SiO_2 catalyst (~ 4wt.% of both Ir and Re) using DRX, TEM, Ir and Re L_3-edge extended X-ray absorption fine structure (EXAFS), XPS and FTIR of adsorbed CO and proposed that the structure of the reduced Ir/ReO_x/SiO_2 had small Ir metal particles of about 2 nm partially covered by 3D clusters of ReO_x. Energy-dispersive X-ray spectroscopy (EDS) was performed over several randomly selected images of Ir/ReO_x/TiO_2 (Figure 3) and the average Re/Ir atomic ratio was 1.1, which is similar to the bulk relationship between both metals and also agrees with the surface Re/Ir ratio estimated from XPS as it will be discuss next.

The nature of the surface species was studied by XPS; samples were previously treated in pure hydrogen at the temperature of the first reduction peak determined by TPR for Ir/ReO_x/support catalysts. In addition, the samples were treated *in situ* using 5%H_2/Ar at the same temperature in the XPS unit. Figure 4 and 5 show the XPS spectra in the Ir 4f and Re 4f regions respectively and a remarkable difference in the oxidation states of both metals when changing the support can be appreciated. Figure 4 reveals the presence of three oxidation states of Ir on the surfaces: Ir^0, Ir^{+III} or Ir^{+IV}; the binding energy for $4f_{7/2}$ for Ir^0, Ir^{+III} and Ir^{+IV} widely accepted in literature are 60.6 eV, 61 eV and 62.5 eV, respectively[57]. The analysis of the spectra corresponding to the Re 4f signals (Figure 5), displayed five doublets ($4f_{7/2}$ and $4f_{5/2}$), where each doublet corresponds to a Re species between Re^{+VII} and Re^0. The characteristic binding energies as reported in bibliography[58,59] are 40 eV (Re^0), 42 eV (Re^{+IV}), 43.5 eV (Re^{+V}), 44.8 eV (Re^{+VI}) and 46.5 eV (Re^{+VII}). Regarding the support, the XPS regions Si2p for Ir/ReO_x/SiO_2, Al2p for Ir/ReO_x/Al_2O_3, Ce3d for Ir/ReO_x/CeO_2, Ti2p for Ir/ReO_x/TiO_2 and Zr3d for Ir/ReO_x/ZrO_2 are shown in Figure S.3 (Supporting Information). The only catalyst that exhibited some modification of the support with catalyst pretreatment was Ir/ReO_x/CeO_2. Actually, both oxides can be detected in the XPS spectrum: CeO_2 (Ce^{+IV}) and Ce_2O_3 (Ce^{+III}) thereby endorsing the reduction of some ceria in good agreement with the TPR results in Figure 2 and Table 2.

The spectra were processed in order to obtain the distribution of species of Ir and Re on each catalyst surface and the results are shown in Table 4. Ir was mainly in metallic state for all the catalysts; the Ir^0 content ranged between 57% (Ir/ReO_x/TiO_2) and ≈ 80 % (Ir/ReO_x/SiO_2 and Ir/ReO_x/AC). All the solids displayed some Ir^{+III} species whereas Ir^{+IV} was only detected on reducible supports. In good agreement to TPR results, the distribution of Re species was different depending on the support used. Some Re^0 was identified when using non-reducible supports (between 20 and 37% of Re^0 on SiO_2, Al_2O_3 and AC); however, Re^{+V} was the predominant species on Ir/ReO_x/AC and Re^{+VI} on Ir/ReO_x supported on SiO_2 and Al_2O_3. On the contrary, the Re^0 content was low on reducible supports; the predominant surface species of rhenium on Ir/ReO_x/TiO_2 was Re^{+IV}, while in the case of Ir/ReO_x/ZrO_2 the predominant species were Re^{+V}.

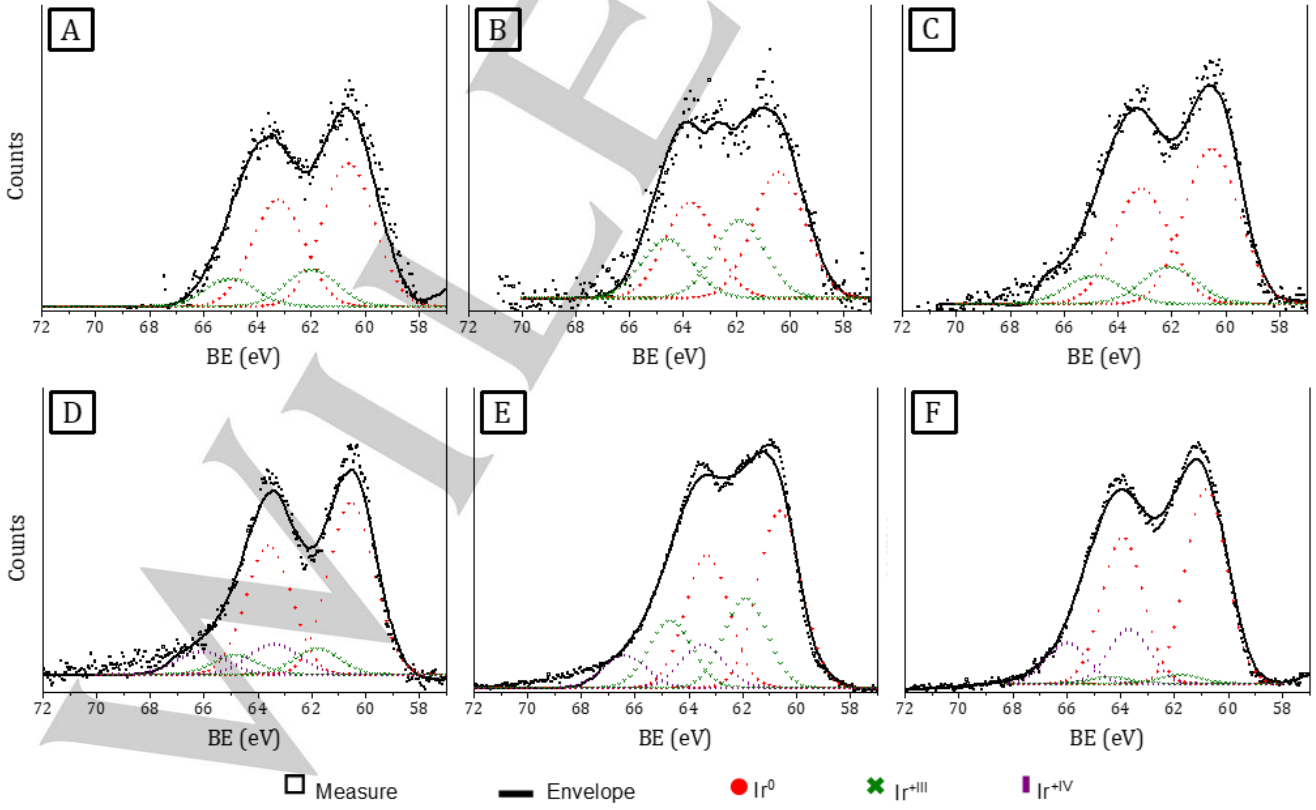

Figure 4. XPS spectra of Ir4f región of (A) Ir/ReO_x/SiO_2, (B) Ir/ReO_x/Al_2O_3, (C) Ir/ReO_x/AC, (D) Ir/ReO_x/CeO_2, (E) Ir/ReO_x/TiO_2 and (F) Ir/ReO_x/ZrO_2.

The presence of Re species partially reduced is in good agreement with the stabilization of rhenium species at intermediate oxidation states in bimetallic catalysts as previously reported[60]. Moreover, redox support such as ceria, zirconia or titania are able to avoid the over-reduction of Re species by the interaction between Re species and the CeO_2, ZrO_2 or TiO_2 surface[61]. Summarizing, the nature of support and the reduction temperature of the samples strongly influence on the preponderant oxidation state of both the Ir and Re surface species and therefore, the six catalysts prepared in this work displayed different surface properties.

Table 4 also shows the molar ratio between Re and Ir in the bulk $(Re/Ir)_{bulk}$ and in the surface $(Re/Ir)_{surface}$ calculated from the chemical composition in Table 1 and XPS measurements, respectively. $(Re/Ir)_{surface}/(Re/Ir)_{bulk}$ was higher than 1 on Ir/ReO_x supported on Al_2O_3, SiO_2 and ZrO_2, close to 1 when using TiO_2 and CeO_2 and lower than 1 in the case of Ir/ReO_x/AC.

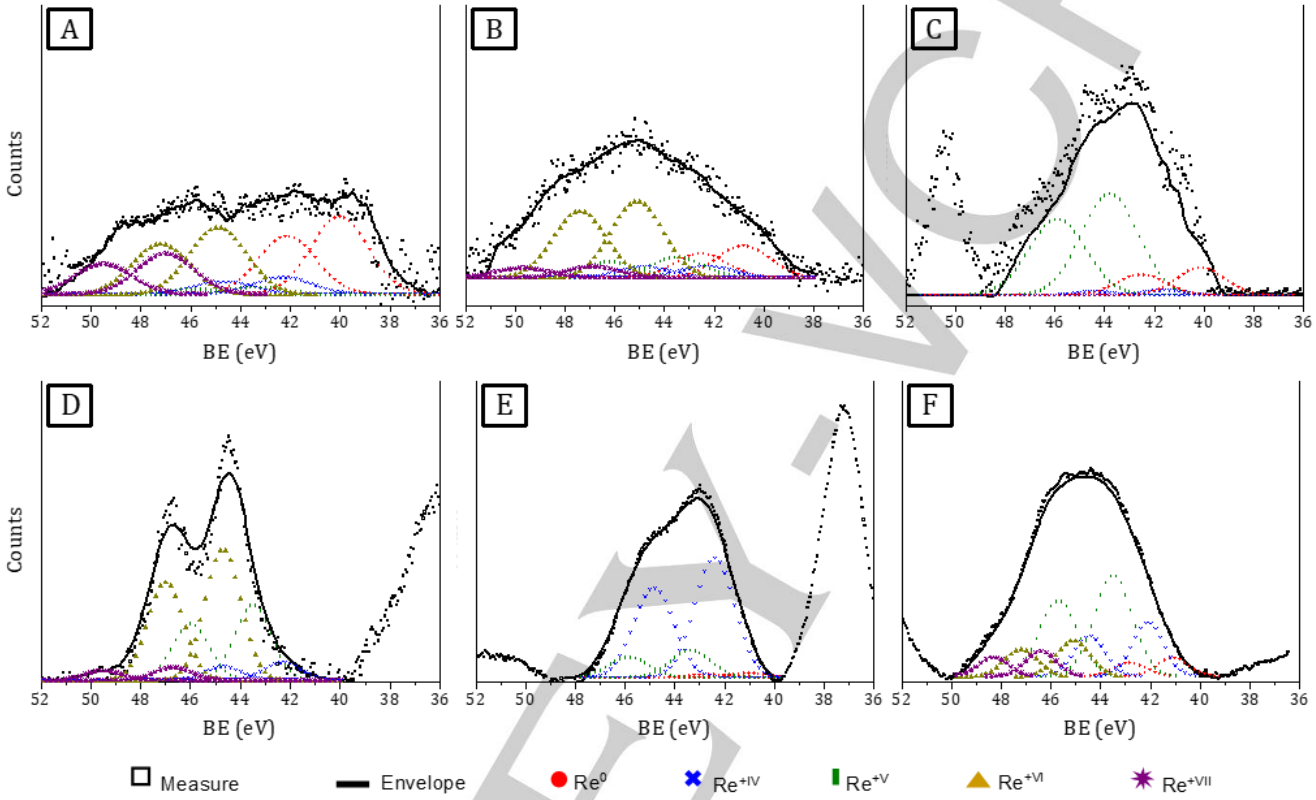

Figure 5. XPS spectra of Re4f región of (A) $Ir/ReO_x/SiO_2$, (B) $Ir/ReO_x/Al_2O_3$, (C) Ir/ReO_x/AC, (D) $Ir/ReO_x/CeO_2$, (E) $Ir/ReO_x/TiO_2$ y (F) $Ir/ReO_x/ZrO_2$.

Table 4. XPS results.

Catalyst	Ir species (%)			Re species (%)					Bulk	Surface	Coverage[a]
	Ir^0	Ir^{+III}	Ir^{+IV}	Re^0	Re^{+IV}	Re^{+V}	Re^{+VI}	Re^{+VII}	$(Re/Ir)_B$	$(Re/Ir)_S$	(%)
$Ir/ReO_x/SiO_2$	80	20	0	37	8	3	32	20	0.8	1.2	68
$Ir/ReO_x/Al_2O_3$	62	38	0	20	2	4	74	0	1.0	1.6	41
Ir/ReO_x/AC	79	21	0	29	10	61	0	0	1.4	0.6	39
$Ir/ReO_x/CeO_2$	74	11	15	0	7	32	56	5	1.2	0.9	38
$Ir/ReO_x/TiO_2$	57	29	14	3	79	18	0	0	1.2	1.2	42
$Ir/ReO_x/ZrO_2$	75	4	21	7	20	48	15	10	0.8	1.6	51

[a] Surface coverage of ReO_x on Ir metal = % coverage = $\left(1-\frac{D_{CO}\times Ir^0}{\frac{1.1}{d_{pTEM}}}\right)\cdot 100$.

The surface coverage ratio of ReO_x on Ir metal surface was also estimated according to literature[22] as % coverage $= [1 - (D_{CO} \times Ir^0)/(1.1/d_{pTEM})] \cdot 100\%$ and values are reported in Table 4. The coverage ratio was 38-42% for Ir/ReO_x supported on Al_2O_3, AC, CeO_2 and TiO_2 whereas it was 51% and 68% for Ir/ReO_x/ZrO_2 and Ir/ReO_x/SiO_2 respectively. Thus, the high coverage value reported for Ir/ReO_x/SiO_2 would be in good agreement with the presence of ReO_x clusters on Ir metal particles proposed from CO chemisorption results in conjunction with TEM results showing that part of Ir was inaccessible to CO.

Proposal of surface models

The different surface properties of Ir/ReO_x supported on solids with well-differentiated characteristics can be explained taking into account the catalysts surface area, $(Re/Ir)_{bulk}$ vs $(Re/Ir)_{surface}$, Ir dispersion, physicochemical properties of the support and the oxidation state of both Ir and Re. Scheme 1 proposes a model of the Ir and ReO_x distribution on the six supports considering the results of the characterization techniques discussed previously and information from literature[22,56,62]. Ir/ReO_x/SiO_2, Ir/ReO_x/Al_2O_3 and Ir/ReO_x/AC displayed moderate-high surface area (269, 218 and 692 g/m^2 respectively) while the surface area was lower than 85 m^2/g for catalysts based on CeO_2, TiO_2 and ZrO_2. Results from XPS suggested that some catalysts surfaces were enriched with Re such as Ir/ReO_x on Al_2O_3, SiO_2 and ZrO_2 while the $(Re/Ir)_{bulk}$ was similar to $(Re/Ir)_{surface}$ when using TiO_2 and CeO_2 but higher in the case of Ir/ReO_x/AC (Table 4). Therefore, if $(Re/Ir)_{surface}/(Re/Ir)_{bulk} > 1$, some Re clusters [63,64] would be probably covering the Ir clusters (coverage > 50%, catalysts supported on SiO_2 and ZrO_2); in contrast, some segregated clusters of Re species would cause $(Re/Ir)_{surface}/(Re/Ir)_{bulk} < 1$ as in the case of Ir/ReO_x/AC in good agreement with TPR profile for this solid (ΔT_{TPR}≈100 K) . Furthermore, results from XPS measurements also indicated that Re species were found as Re^0 only when using non reducible supports (SiO_2, Al_2O_3 and AC) while Re^{+IV}, Re^{+V} and Re^{+VI} prevailed on Ir/ReO_x supported on TiO_2, ZrO_2 and CeO_2, respectively. The close contact of both Ir and ReO_x species on CeO_2, TiO_2 and ZrO_2 can be also deduced from the proximity of their assigned peaks of reduction in TPR profiles ($\Delta T_{TPR} \leq 60$ K). On the other hand, results from CO chemisorption and TEM showed the highest Ir dispersion and, in consequence, the lowest particle diameter on Ir/ReO_x/CeO_2; particles lower than 2 nm were detected for Ir/ReO_x on TiO_2, Al_2O_3 and AC while particles were higher than 3 nm for Ir/ReO_x/SiO_2 and Ir/ReO_x/ZrO_2. The difference between the particle diameters estimated by CO chemisorption and TEM for Ir/ReO_x/SiO_2 and the high coverage of Ir with ReO_x clusters (Table 4) strongly suggests that some Ir was not accessible to CO probably because it was covered by ReO_x.

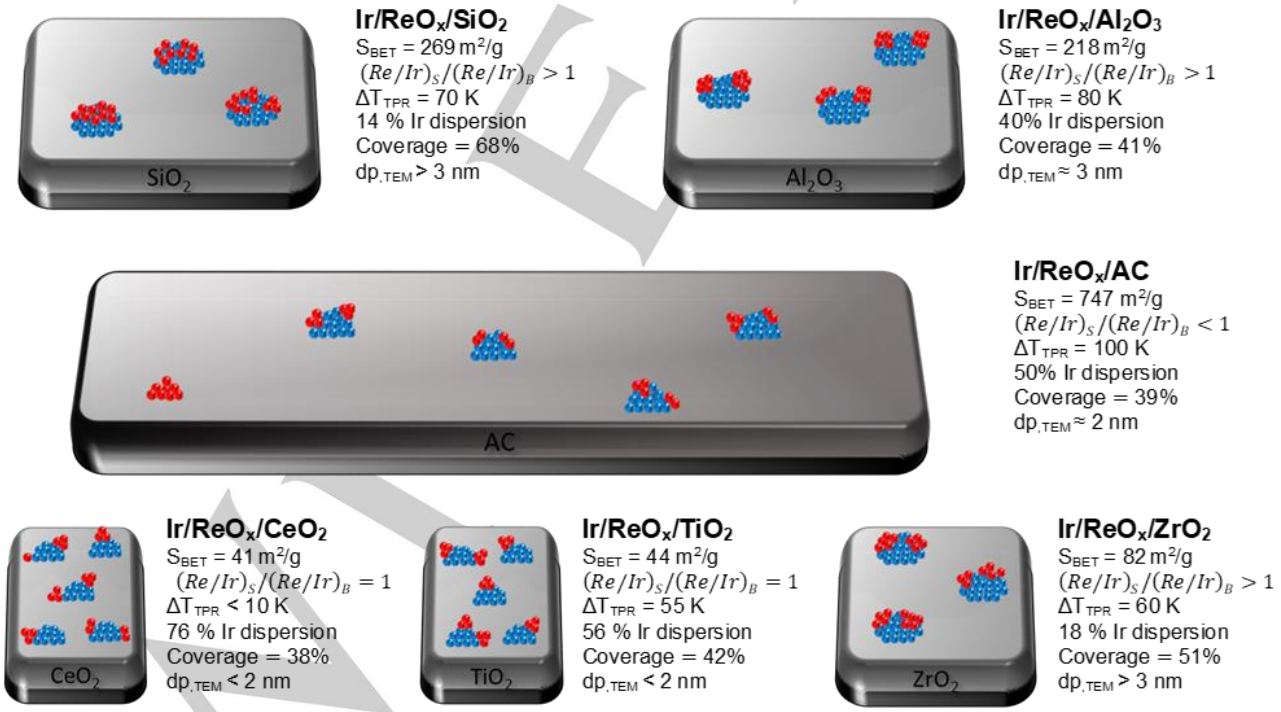

Scheme 1. Schematic illustration of the surfaces of the different catalysts (blue: Ir, red: Re).

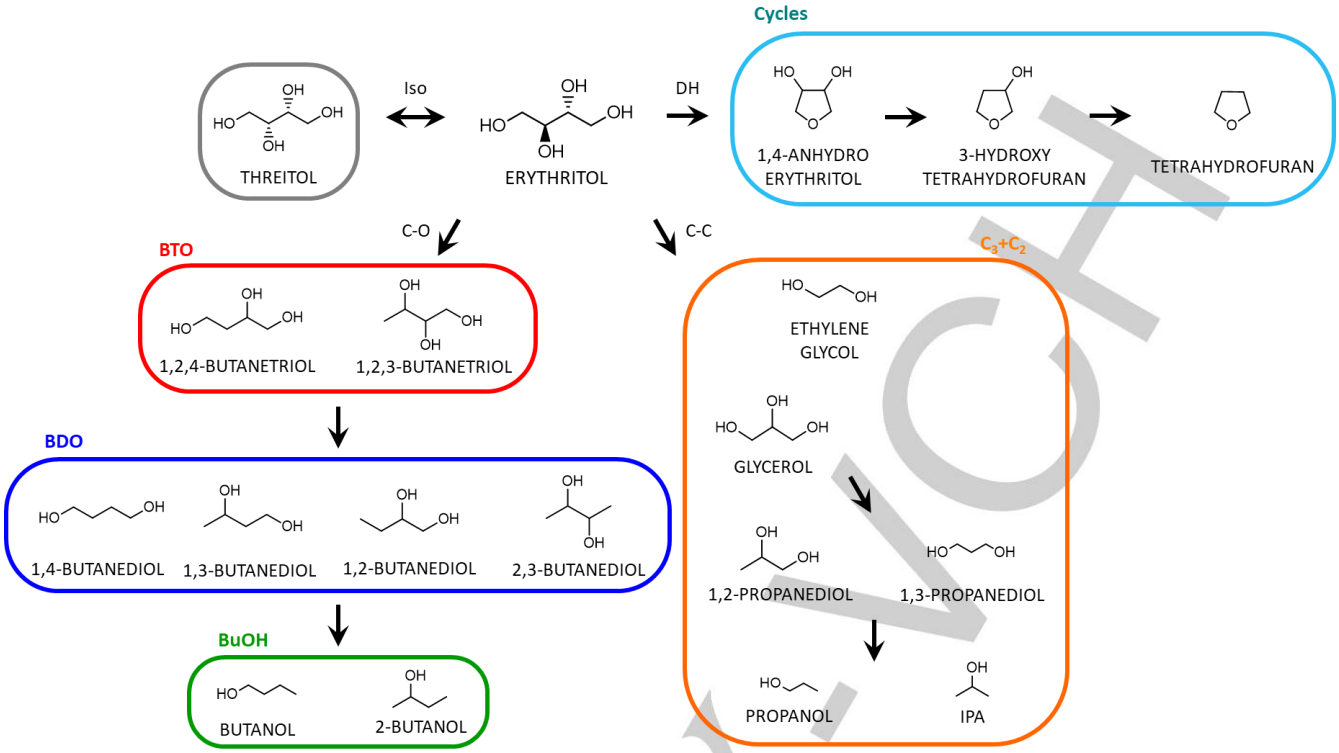

Scheme 2. Reaction network for erythritol under hydrogenolysis conditions.

Catalytic tests

Reaction network for erythritol under hydrogenolysis conditions and preliminary catalytic results

Erythritol reacts in the presence of H_2 and a metal/support catalyst to give numerous products as shown in Scheme 2. The primary routes involve the formation of: 1,4 anhydroerythritol (1,4AE) by dehydration, glycerol (GLY) and ethylene glycol (EG) by C-C cleavage, butanetriols (BTO) by C-O scission and finally, ERY may isomerize to threitol (TRE). A subsequent C-O hydrogenolysis of BTO allows obtaining butanediols (BDO) and butanols (BuOH, including n-butanol and isobutanol) which by further dehydration and hydrogenation or C-O hydrogenolysis produce butane and isobutane. On the other hand, the loss of hydroxyl groups of 1,4AE lead to formation of 3-hydroxytetrahydrofuran (3OTHF) and tetrahydrofuran (THF) whereas consecutive hydrogenolysis of ethylene glycol and glycerol may form ethanol (EtOH) and C3 products such as 1,3 propanediol (13PDO), 1,2-propanediol (12PDO), propanol (PrOH) and isopropanol (IPA), respectively.

The first C-O hydrogenolysis of ERY produces 1,2,3BTO and 1,2,4BTO and subsequent C-O cleavage of these products yields the four butanediol isomers (1,2BDO, 1,3BDO, 2,3BDO and 1,4BDO). It is important to note here that 1,4BDO and 2,3BDO only come from 1,2,4BTO and 1,2,3BTO, respectively, whereas 1,2-BDO and 1,3BDO may be produced from both BTO. Other authors have suggested that butanediols can also be formed directly from ERY by a double C-O hydrogenolysis over Rh-based catalysts[39] or by simultaneous hydrodeoxygenation which removes two vicinal OH groups on Pd-ReO_x/CeO_2[65].

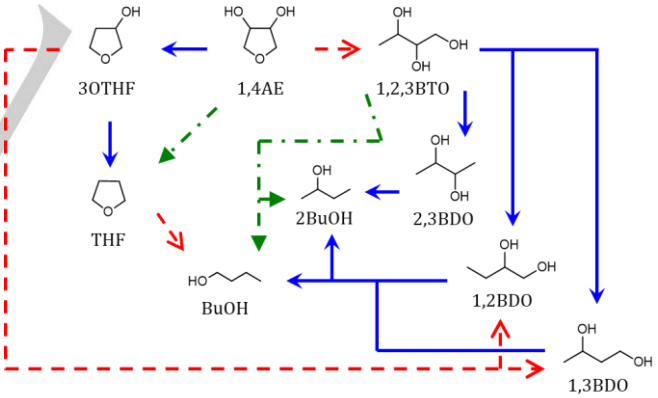

Scheme 3. Butanediols formation from 1,4AE. (→) Simple C-O Hydrogenolysis, (⇢) Double C-O Hydrogenolysis and (⇢) Ring Opening.

Additionally, 1,2BDO, 2,3BDO and 1,3BDO can be generated from 14AE according to Scheme 3[39,66].

Preliminary reactions without solid catalysts or H_2SO_4, with minimal amount of H_2SO_4 or using only the support were conducted at 473 K, 25 bar H_2 and erythritol initial concentration (C^0_{ERY}) of 0.4 M. In absence of catalyst and acid, the erythritol conversion (X_{ERY}) was null and no products were detected, the carbon balance was 99% after 6 h of reaction. ERY was, however, transformed into 1,4AE ($C_{1,4AE}$=55 mM) reaching a

X_{ERY}≅14 % when a minimal amount of H_2SO_4 was added (1.5 µl for 40 cm^3 of liquid). Experiments using SiO_2, Al_2O_3, AC, CeO_2, TiO_2 and ZrO_2 (C_{cat}=0.0125 g/cm^3) were performed during 6 h and ERY conversion lower than 6 % was achieved except for CeO_2 and AC (X_{ERY}≅14 and 50% respectively at 6 h). 1,4AE was the only liquid product formed and gaseous products were not detected. The carbon balance (CB) was close to 100%, except for CeO_2 and AC (CB ≅ 88 and 50% respectively). These low CB value for AC (support with highest S_{BET} according to Table 1) and in less extent on CeO_2, can be explained by a strong adsorption of ERY.

Effect of the support on erythritol conversion and products distribution

Catalytic tests were performed using the six Ir/ReO_x supported catalysts at 473 K, 25 bar of H_2, C^0_{ERY} = 0.4 M, C_{cat} = 0.0125 g/cm^3 and 1.5 µL of H_2SO_4. Since, it is well known that some of rhenium oxides such as Re_2O_7 and ReO_3 are soluble in water[54] the Re content was analyzed in the liquid recovered from reactions verifying that Re leaching was no significant for these reactions conditions. Indeed, inductively coupled plasma (ICP) analysis of the reaction solution showed an undetected leaching of both Ir and Re (<0.01 % for each metal).

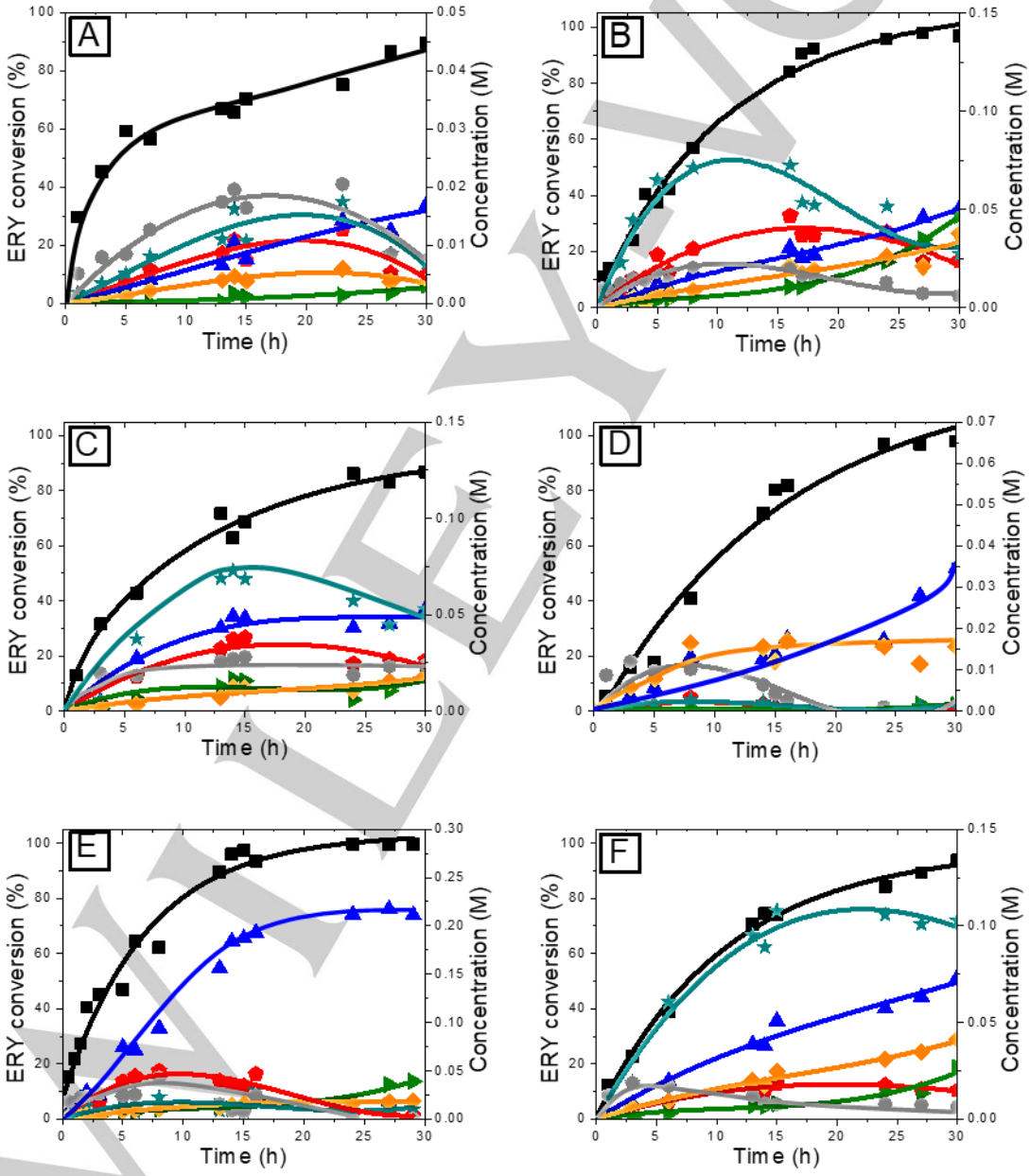

Figure 6. Erythritol conversion and products concentrations as a function of reaction time. (A) Ir/ReO_x/SiO_2, (B) Ir/ReO_x/Al_2O_3, (C) Ir/ReO_x/AC, (D) Ir/ReO_x/CeO_2, (E) Ir/ReO_x/TiO_2, (F) Ir/ReO_x/ZrO_2. (■) X_{ERY}, (⬟) BTO, (▲) BDO, (▶) BuOH, (★) Cycles, (◆) C_3+C_2, (●) TRE [473K, P_{H2}=25bar, C^0_{ERY}=0.4 M, C_{cat}=0.0125 g/cm^3, W_{cat} =0.5 g].

The temporal evolution of ERY conversion and product concentrations shown in Figure 6 A-F indicated that X_{ERY} was at least 70% after 15 h reaction and higher than 85% at 30 h reaction. Almost total conversion was achieved on Ir/ReO_x/Al_2O_3, Ir/ReO_x/CeO_2 and Ir/ReO_x/TiO_2 at 30 h. The product distribution significantly varied when changing the support (Figure 6). It is important to note that the total liquid products concentrations on Ir/ReO_x/TiO_2, Ir/ReO_x/ZrO_2, Ir/ReO_x/AC and Ir/ReO_x/Al_2O_3 were higher than on Ir/ReO_x/CeO_2 and Ir/ReO_x/SiO_2 (see Y-axis scale on Figure 6). We will first analyze the results on Ir/ReO_x/SiO_2 catalyst considering the SiO_2 as the most inert support used here since it has no redox properties and very low acidity according the results in Table 1. The main products observed during the first 20 h of reaction using Ir/ReO_x/SiO_2 (Figure 6A) were threitol (erythritol isomer), cyclic products, BTO and BDO. Threitol was formed directly from ERY and its concentration reached a maximum and then decreased suggesting that this C4 polyol could isomerize to ERY motivated by the high consume of the reactant considering the low reactivity of TRE as it was informed previously [39] and therefore its conversion to other products could be discarded. Products from dehydration reactions (cycles) were also significantly formed on this catalyst, the cycles concentration (C_{cycles}) curve went through a maximum at 20 h and included almost exclusively 1,4AE formed by direct dehydration of the reactant (Figure S.4., Supporting Information). BTO were formed as primary products by the first C-O hydrogenolysis of ERY and then were transformed into BDO, as suggested by the maximum in its curve at 22 h of reaction, by a further C-O hydrogenolysis in good agreement with the reaction network proposed in Scheme 2. BDO concentration monotonically increased with time to reach the highest concentration at the end of reaction (30 h). Since 1,2BDO, 1,3BDO and 2,3BDO could also come from 14AE (Scheme 3), results from Figure 6A did not allow distinguishing the mechanism for BDO formation at this point. The curve corresponding to the BDO concentration (C_{BDO}) for Ir/ReO_x/SiO_2 did not reach a maximum during the 30 h reaction; however, butanols, the products of a triple C-O hydrogenolysis of ERY, were formed, although, in low proportion. Finally, some products from the scission of C-C bonds (grouped as C2+C3) such as GLY, EG and 13PDO, were also formed in low concentrations.
Ir/ReO_x/TiO_2 was the most active catalyst between the solids tested in this work as evidenced by the high liquid products formation at low reaction time and BDO were the most abundant products during all the 30 h of reaction (Figure 6 E). A maximum BTO concentration of 44 mM (BTO yield: η_{BTO} = 9.6%) was reached at 6 h of reaction and at this time the curve of BDO also presented an inflection point. Unlike Ir/ReO_x/SiO_2, the formation of BDO was clearly predominant on Ir/ReO_x/TiO_2 reaching a maximum concentration of BDO of 212 mM after 24 h of reaction which remained almost constant until 30 h. This corresponds to the highest yield to BDO reported until now (η_{BDO}=53 The C_{BDO} vs time curve seems to have positive slope at $t = 0$, in fact, C_{BDO} during the first 5 h of reaction were higher than C_{BTO} even for $X_{ERY} < 20\%$ suggesting some probable contribution of the direct formation route of this products from ERY. As described above, BDO can be formed: i) from BTO (Scheme 4A) or ii) from ERY direct via a double C-O hydrogenolysis[39] or hydrodeoxygenation (Scheme 4B). Since hydrodeoxygenation on Re species is not usually reported in the aqueous phase some experiments using monometallic ReO_x/supports were performed to get insight on the possibility of BDO formation by this pathway. The catalytic results are informed in Table S2, Supporting Information. Significant amounts of 1,2BDO and 1,4BDO, that are the isomers that can be formed by the elimination of two vicinal OH group, were only formed on ReO_x/TiO_2 whereas BTO were not detected. Thus, hydrodeoxygenation could take place on ReO_x/TiO_2 although it was almost null for the other five supports at the reactions condition used. However, the 1,4BDO concentration was very low when using bimetallic catalyst, as it is shown in the next section, and therefore the hydrodeoxygention would proceed at low rates when comparing to the other routes from ERY suggesting that this mechanism would not be the preponderant route for BDO formation from aqueous solution of ERY on bimetallic samples. The concentration of butanols reached a maximum of 39 mM after 30 h of reaction while the formation of threitol, C2+C3 products as well as 14AE was low on Ir/ReO_x/TiO_2.

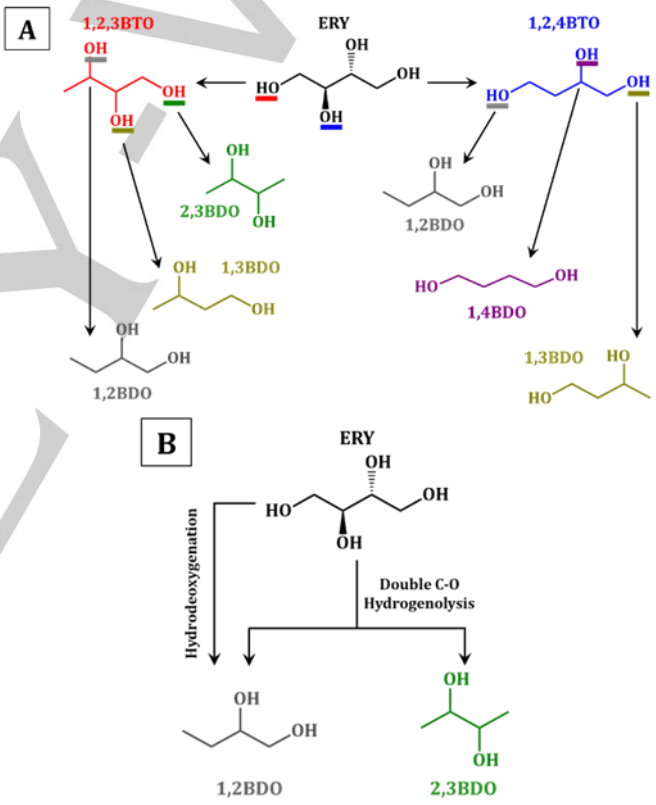

Scheme 4. Butanediols formation via butanetriols (A) or directly from erythritol (B).

The main products formed on Ir/ReO_x/Al_2O_3, Ir/ReO_x/AC and Ir/ReO_x/ZrO_2 catalysts (Figure 6B, C and F) were those grouped as cycles (1,4AE, 3OTHF and THF) from dehydration of ERY and further C-O scissions. It is well known that acid sites promotes dehydration reactions and results of NH_3 TPD shown in Table 1 proved that Ir/ReO_x/Al_2O_3 and Ir/ReO_x/AC were the most acidic catalysts (353 and 252 µmol NH_3/g respectively) whereas Ir/ReO_x/ZrO_2 displayed moderate acidity (84.9 µmol NH_3/g).

1,4AE was the most abundant product within this group for all the catalysts, and the C_{14AE} curves obtained on the three catalysts (Figure S.5., Supporting Information) passed through a maximum indicating that 1,4AE was consecutively transformed into other more volatile products that eventually go to gas phase such as 3OTHF and THF. The C_{cycles}^{max} were 75 mM for $Ir/ReO_x/Al_2O_3$ and Ir/ReO_x/AC and 112 mM for $Ir/ReO_x/ZrO_2$. The formation of BTO and BDO was also observed; C_{BDO} was higher than the C_{BTO} on the three catalysts; the maximum corresponding to the $C_{BTO}\ vs\ time$ curve was achieved approximately at about 15 h for $Ir/ReO_x/Al_2O_3$, $Ir/ReO_x/ZrO_2$ and Ir/ReO_x/AC. The BDO formation route from 1,4AE would not be discarded due to the high $C_{1,4AE}$ on these catalysts (Scheme 3).

Products formed by C-C cleavage, threitol and butanols were also detected but at low concentrations. Finally, $Ir/ReO_x/CeO_2$ mainly formed products from C-C cleavage including glycerol, propanediols and ethylene glycol at reaction times lower than 18h and then, the BDO formation predominated. Similarly to other catalysts, the concentration of threitol curve went through a maximum and became zero after 20 h.

Table 5 shows the carbon balance (CB) at 30 h for the reactions informed in Figure 6 calculated considering the liquid products quantified by HPLC; the ERY conversion and products concentrations at that time are also included. The CB ranged between 60-80%, excepting $Ir/ReO_x/CeO_2$ and $Ir/ReO_x/SiO_2$ whose carbon balances were higher than 80% during the first 6 hours and then rapidly decreased up to ≈ 20% after 30 h reaction. Similar values for carbon balance were previously informed in literature for H_2 pressure close to that used in this work (30 bar) [39]. The formation of gaseous products during ERY reaction cannot be ignored specially when ERY conversion was high (at long reaction times) and significant amounts of volatile products can be formed. The gaseous products distribution for three catalysts with acid and redox properties well-differentiate ($Ir/ReO_x/Al_2O_3$, $Ir/ReO_x/CeO_2$ and $Ir/ReO_x/TiO_2$) is informed in Figure S.5. Supporting Information. Methane and butanol formation were about 30-40% and 20-30%, respectively, of the total gaseous products whereas THF was formed in low concentration. As expected, a 20% of butane was detected on TiO_2 and Al_2O_3 but in minority proportion on CeO_2; products from C-C scission such as propanol were only significant on $Ir/ReO_x/CeO_2$. In spite of some gaseous products formation, the ERY strong adsorption on the catalyst surface should not be discarded as the cause of low CB. The strength of this interaction depends on the nature and properties of catalysts surface since ERY could interact with the support or ReO_x species.

The liquid product distribution at similar erythritol conversion (65%) is compared in Figure 7 to better understand the influence of the nature of the support on the selective butanediol production.

The dehydration reaction to form mainly 1,4AE was promoted on $Ir/ReO_x/Al_2O_3$, $Ir/ReO_x/ZrO_2$ and Ir/ReO_x/AC (the % of cyclic products within liquid products was 47, 50 and 34% respectively) whereas the C-C hydrogenolysis to yield C2+C3 products was favored on $Ir/ReO_x/CeO_2$ but lower than 10% for the rest of the catalysts. The threitol formation was significant for all the solids; nevertheless, its concentration was very low at high ERY conversion. $Ir/ReO_x/TiO_2$ was the most promising solid to selectively improve the C-O hydrogenolysis route showing the highest BTO and BDO formation. Indeed, the amounts of BTO, BDO and butanols within liquid products were 26.6, 43.1 and 4.3%, respectively on $Ir/ReO_x/TiO_2$ (Figure 7). Even though BDO proportion within liquid products was also high when using $Ir/ReO_x/CeO_2$, the carbon balance at 65% ERY conversion was very low (CB = 36%); therefore, the yield to BDO+BTO was only $\eta_{BTO+BDO}$ = 4.4 % compared with $\eta_{BTO+BDO}$ = 21.6 % for TiO_2.

Table 5. Erythritol conversion, products concentrations and carbon balance after 30 h reaction. X_{ERY}: ERY Conversion, CB: Carbon Balance. [30 h reaction, 473 K, P_{H2}=25 bar, C^0_{ERY}=0.4 M, C_{cat}= 0.0125 g/cm^3, W_{cat} =0.5 g]

Catalyst	X_{ERY} (%)	BTO [mmol/L]	BDO [mmol/L]	BuOH [mmol/L]	Cycles [mmol/L]	C3+C2 [mmol/L]	TRE [mmol/L]	CB (%)
$Ir/ReO_x/SiO_2$	89.6	4.9	17.1	3.1	7.1	3.7	7.5	21
$Ir/ReO_x/Al_2O_3$	96.7	23.8	49.9	97.2	27.1	37.5	5.7	80
Ir/ReO_x/AC	86.9	26.4	52.8	19.4	52.7	18.2	23.6	62
$Ir/ReO_x/CeO_2$	97.9	0	34.6	1.6	1.3	15.5	0.3	20
$Ir/ReO_x/TiO_2$	99.6	3.8	211.0	39.0	10.2	18.6	0.4	71
$Ir/ReO_x/ZrO_2$	93.7	4.9	71.1	3.1	7.1	3.7	7.5	73

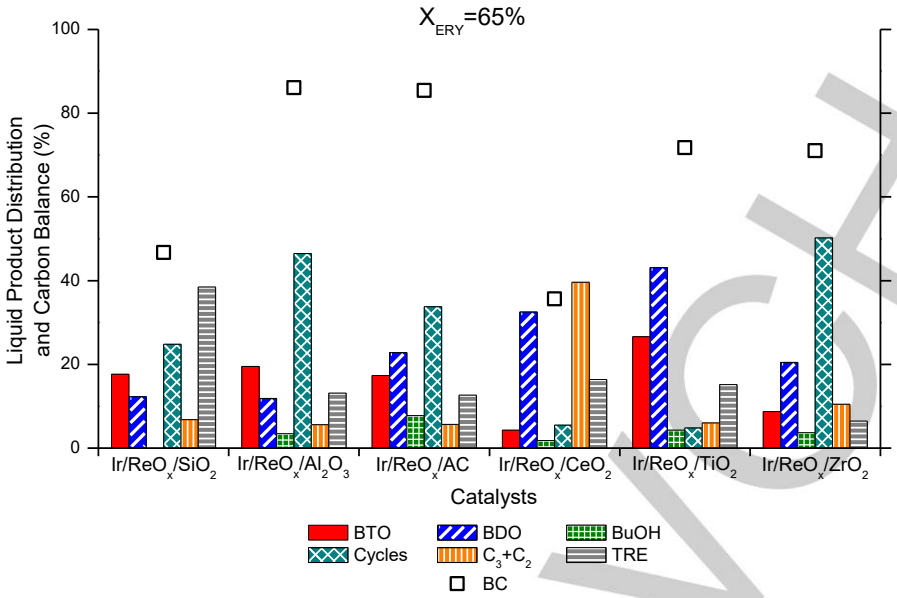

Figure 7. Liquid products distribution and carbon balance for 65 % of erythritol conversion [473 K, P_{H2}=25 bar, C^0_{ERY}=0.4 M, C_{cat}=0.0125 g/cm^3, W_{cat} =0.5 g].

Table 6. Turnover frequency for erythritol reactions on Ir/ReOx/support catalysts. C-O: C-O Hydrogenolysis, C-C: C-C Hydrogenolysis. [473 K, P_{H2}=25 bar, C^0_{ERY}=0.4 M, C_{cat}= 0.0125 g/cm^3, W_{cat} =0.5 g]

Catalyst	TOF (mmol/mmol$_{IrS}$ min)		
	$TOF_{C\text{-}O}$	$TOF_{C\text{-}C}$	$TOF_{C\text{-}O}$ / $TOF_{C\text{-}C}$
Ir/ReO$_x$/SiO$_2$	226.5	58.0	3.9
Ir/ReO$_x$/Al$_2$O$_3$	432.2	20.0	21.6
Ir/ReO$_x$/AC	190.8	16.0	11.9
Ir/ReO$_x$/CeO$_2$	39.4	43.0	0.9
Ir/ReO$_x$/TiO$_2$	499.1	29.5	16.9
Ir/ReO$_x$/ZrO$_2$	573.2	133.7	4.3

On Ir/ReO$_x$/SiO$_2$ the carbon balance was also poor (CB = 47%) whereas ranged between 72 and 87 % for the other catalysts.

The initial turnover frequency (expressed as mmol i product/mol$_{Ir\ Sup}$.min) for the reactions catalyzed by Ir, i.e. C-O (TOF_{C-O}) and C-C hydrogenolysis (TOF_{C-C}) are informed in Table 6. The route involving C-O scissions was clearly promoted on Ir/ReO$_x$ supported on ZrO$_2$, TiO$_2$ and Al$_2$O$_3$ (TOF_{C-O} = 573.2, 499.1 and 432.2 mmol/mol$_{IrSup}$.min respectively). Ir/ReO$_x$/ZrO$_2$ displayed the highest TOF for reactions involving C-C scissions (133.7 mmol/mol$_{IrSup}$.min). The C-O/C-C hydrogenolysis ratios (TOF_{C-O}/TOF_{C-C}) were also reported in Table 6; this ratio was especially high on Ir/ReO$_x$/TiO$_2$ and Ir/ReO$_x$/Al$_2$O$_3$ (16.9 and 21.6 respectively) whereas it was lower than 1 on Ir/ReO$_x$/CeO$_2$ indicating the preferential C-C scissions route on this catalyst.

BTO and BDO isomers distribution

The temporal evolution of BTO and BDO isomers concentrations are displayed in Figure 8 (A-F). 1,2,3BTO and 1,2,4BTO curves were similar for any time when using Ir/ReO$_x$ supported on SiO$_2$, Al$_2$O$_3$, AC and ZrO$_2$ while the formation of 1,2,4BTO was significantly higher than the 1,2,3BTO on TiO$_2$ and CeO$_2$. However, the initial formation rate of both BTO isomers was almost identical ($r^0_{1,2,4BTO}/r^0_{1,2,3BTO} \approx 1$) for Ir/ReO$_x$/TiO$_2$ suggesting that there is not preferential removing of the primary or secondary OH group of ERY as previously informed using Rh/ReO$_x$/TiO$_2$[39]. The BTO concentration curves went through a maximum (see also Figure 6 E) indicating their further conversion to BDO. The time to reach this maximum was always lower for the 1,2,3BTO curve than for 1,2,4BTO that would probably indicate the highest reactivity of 1,2,3BTO towards C-O hydrogenolysis. However, experiments using both triols as reactants on Rh/ReO$_x$/TiO$_2$ at 473 K and 80 bar H$_2$[39] and Ir/ReO$_x$/SiO$_2$ at 373-393 K and 120 bar H$_2$[41] indicated that 1,2,4BTO hydrogenolysis proceeded more rapidly than the reaction of 1,2,3BTO under the same conditions and it was attributed to the ability of 1,2,4BTO to form cyclic ethers such as 3OTHF and THF while 1,2,3BTO cannot be dehydrated to form that cycles[39]. Nevertheless, cyclic ethers were not formed in significant proportions on the catalysts at the reaction conditions reported here.

Regarding BDO isomers, it can be appreciated that 1,2BDO was predominantly formed followed by 2,3BDO, while 1,3BDO and 1,4BDO concentrations were always low except on Ir/ReO$_x$/TiO$_2$. Actually, the 2,3BDO formation was promoted on TiO$_2$ based catalyst and also significant amount of 1,2BDO and 1,3BDO were detected. Similarly, both 1,2BDO and 2,3BDO were the main diols formed on sulfur-modified ruthenium catalysts at 513 K and 40 bar H$_2$[26] and when using Rh/ReO$_x$/TiO$_2$ at 473 K and 80 bar H$_2$[39] while only a minimal amount of the other isomers were detected. However, Tomishige et al. have recently reported[40] the preferential formation of 1,4BDO and to a lesser extent 1,3BDO on Ir/ReO$_x$/rutile at 373 K and 80 bar H$_2$; the discrepancy in the isomers distribution could be related to the different reaction temperature[39].

The temporal evolution of the concentration curves displayed in Figure 8 would indicate that the 1,2BDO initial formation rate was null for Ir/ReO_x on SiO_2, Al_2O_3 and AC and therefore, it would be formed from 1,2,3BTO or 1,2,4BTO. Actually, 1,2,4BTO can yield 1,2, 1,3 and 1,4BDO isomers but, according to the catalytic results, 1,2BDO would be the most favored isomer in good agreement with results previously reported proving the superior reactivity of the OH group in the 4-position that has less steric hindrance[39]. On the contrary, 1,2BDO was rapidly formed from the beginning of reaction on Ir/ReO_x supported on CeO_2, TiO_2 and ZrO_2 suggesting some contribution of a direct route from ERY (Scheme 4 B) as it will be discussed later. In addition, some contribution to 1,2BDO formation from 1,4AE according the Scheme 3 could not be discarded on catalysts that significantly formed this dehydration product from ERY (Al_2O_3, AC and ZrO_2).

The 2,3BDO formation was also significant on all the solids; however, its initial formation rate was null for all the catalyst except Ir/ReO_x/TiO_2. Since reactivity of terminal OH group in the 1-position of 1,2,3BTO has been claimed to be higher than that of the secondary OH group[39], 2,3 BDO would be the main product from 1,2,3BTO. Even though, in the case of Ir/ReO_x supported on TiO_2, considering that 2,3BDO cannot be formed from 1,2,4BTO, the low concentration of 1,2,3BTO observed and the nonzero slope a t=0 of the $C_{2,3BDO}$ vs time curve, a direct route from ERY should also be considered.

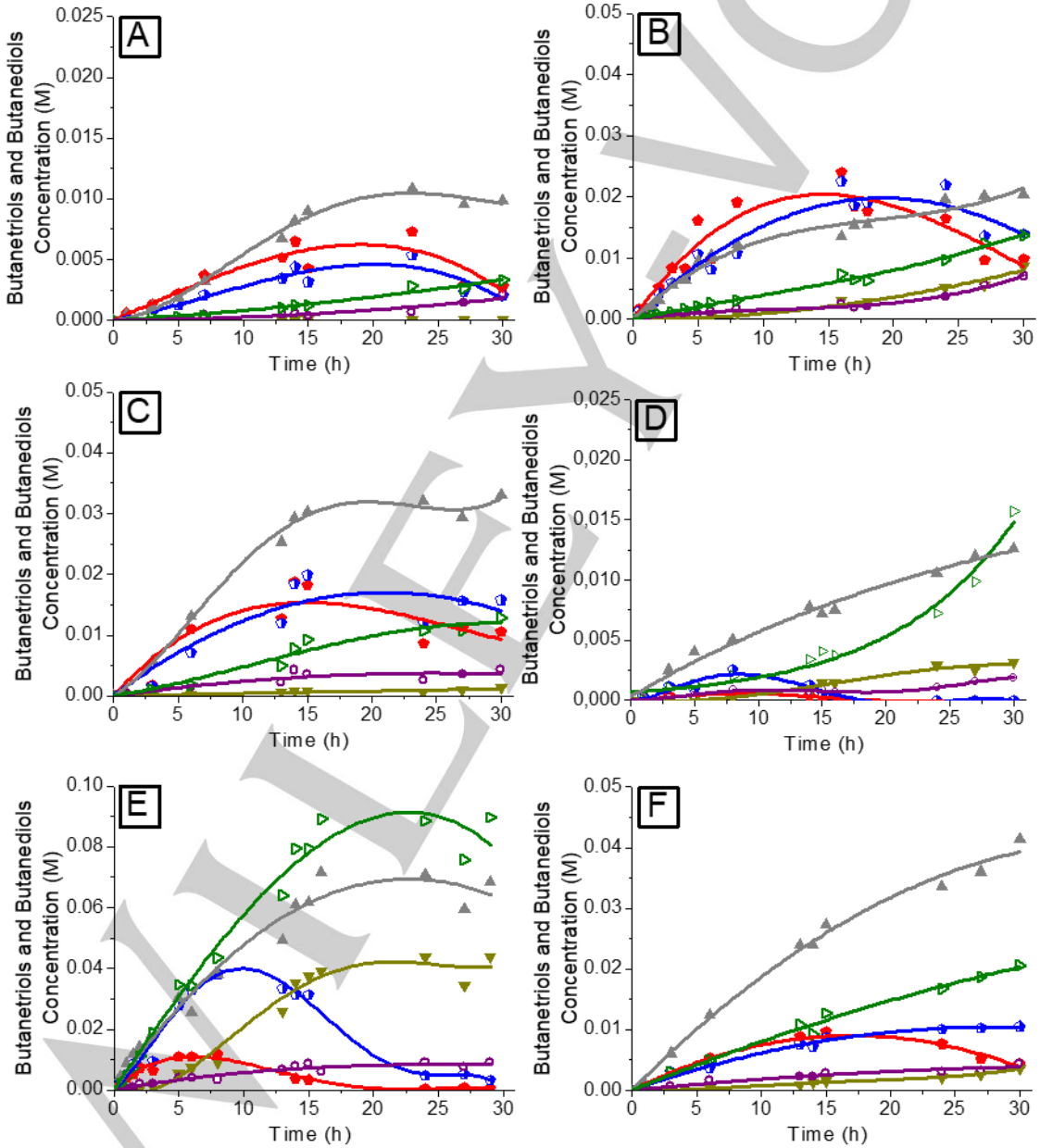

Figure 8. BTOs and BDOs concentrations as a function of reaction time. (A) Ir/ReO_x/SiO_2, (B) Ir/ReO_x/Al_2O_3, (C) Ir/ReO_x/AC, (D) Ir/ReO_x/CeO_2, (E) Ir/ReO_x/TiO_2, (F) Ir/ReO_x/ZrO_2, (⬟) 1,2,3BTO, (◓) 1,2,4BTO, (▲) 1,2BDO, (▼) 1,3BDO, (◎) 1,4BDO, (▶) 2,3BDO, [473 K, P_{H2}=25 bar, C^0_{ERY}=0.4 M, C_{cat}=0.0125 g/cm^3, W_{cat} =0.5 g].

1,3BDO formation was only noticeable on $Ir/ReO_x/TiO_2$; 1,3BDO concentration curve on this solid showed a zero initial slope and an inflection point when 1,2,4BTO curve reached the maximum concentration indicating that 1,3BDO would be mainly formed from the elimination of a primary OH group in C1 of 1,2,4BTO. 1,4BDO was the least abundant isomer on all the catalysts probably because its formation would involve the less favored elimination of a secondary OH group of 1,2,4BTO. The 1,3BDO and 1,4BDO formation pathways proposed here are consistent with catalytic results on $Rh/ReO_x/TiO_2$ at 473 K[39] but differ from previously results over $Ir/ReO_x/SiO_2$ at 373 K[41] and Ir/ReO_x/rutile at 353 K[40] since low reaction temperature seems to favor preferential formation of 1,3BDO and 1,4BDO from 1,2,3BTO and 1,2,4BTO respectively.

Relationship between catalyst surface properties and catalytic activity

The different catalytic behavior of Ir/ReO_x supported catalysts with well-differentiated characteristics can be explained taking into account the surface models proposed in Scheme 1. The supports of $Ir/ReO_x/Al_2O_3$ and Ir/ReO_x/AC displayed high surface area and density of acid sites that being mostly exposed would promote the dehydration of ERY (Figure 6B and C)[67]. Furthermore, ReO_x species could increase the acidity of the support as previously reported for ReO_x supported on Al_2O_3; rhenium oxide would deposit preferentially on the weak Lewis sites and this deposition turns them into stronger Lewis sites[68]. Moreover, Brønsted acidity has been attributed to Re-OH sites near to noble metal on bimetallic catalyst[69]. Thus, the 1,4AE formation could take place on acid sites from both the support and Re species. $Ir/ReO_x/ZrO_2$ also selectively promoted the dehydration reaction as shown in Figure 6F and Figure 7. Although, $Ir/ReO_x/ZrO_2$ and $Ir/ReO_x/TiO_2$ have similar acid sites concentration, the difference in surface area and Ir dispersion (Table 1 and Table 3) suggest that acid sites of ZrO_2 or acidic Re species would be more accessible than on TiO_2 (Scheme 1) favoring dehydration reactions. The higher formation of C2+C3 products on $Ir/ReO_x/ZrO_2$ when it is compared to $Ir/ReO_x/TiO_2$ could be related to the highest particle size for $Ir/ReO_x/ZrO_2$ (Table 3) that would favor the structure-sensitive C-C hydrogenolysis reaction[70,71]. Although it is well known that Ir^0 is necessary for activating H_2 involved in the C-O hydrogenolysis, high Ir clusters would be not appropriate to selectively produce BDO since the undesirable C-C scission would be favored. The low liquid products concentrations achieved on $Ir/ReO_x/SiO_2$ and $Ir/ReO_x/CeO_2$ could be also explained considering the strong adsorption of ERY on ReO_x clusters or the support, mainly on CeO_2, and the hydrogenolysis to gaseous products (Figure S6 Supporting Information) resulting in a poor carbon balance for high reaction times (Table 5).

The most active and selective catalyst towards BDO formation was $Ir/ReO_x/TiO_2$ (maximum BDO yield = 53% at 24 h) and this particular behavior would be attributed to the moderate acidity and surface area of TiO_2 and the close contact between Ir^0 and ReO_x species with Re partially oxidized, mainly present as Re^{+IV} (Table 4). These results along with previous papers dealing with the role of ReO_x in this type of catalysts[22] lets conclude that the formation of BDO requires the presence of Ir^0, but it is also necessary that the Re be partially oxidized in intimate contact with Ir clusters. Metallic Re or more oxidized Re species did not selectively lead to the desired route, as is the case of CeO_2, SiO_2, AC and Al_2O_3.

It is worth mentioning that 2,3BDO and 1,2BDO were the main isomers formed on the six catalysts tested in this work in accordance with results on Rh based catalysts at the same reaction temperature[42]. In fact, after 24 h of reaction at 473 K on $Ir/ReO_x/TiO_2$, the yield to each individual BDO isomers were 2,3BDO: 22.3%, 1,2BDO: 17.5%, 1,3BDO: 11.1% and 1,4BDO: 2.1% whereas on Rh/ReO_x catalysts the maximum yields reported were 12.3% 1,2BDO, 14.1% 2,3BDO, 2.6% 1,4BDO and 0% 1,3BDO[42]. On the contrary, Gu et al.[40], reported that at 373 K and H_2 pressure of 80 bar over 4%wt Ir/1%wt ReO_x/TiO_2 the main BDO obtained was 1,4BDO, reaching after 24 h of reaction a maximum yield of 23 % (total BDO yield of 25%). Furthermore, the maximum productivity informed for 4%wt. Ir/1%wt.ReO_x/TiO_2 at the mentioned conditions was 25.5 mmol/g_{Ir} h at 4 h of reaction (1,4BDO productivity: 20 mmol 1,4BDO/g_{Ir} h)[40], while the maximum productivity reported here was 60 mmol BDO/g_{Ir} h at 5 h of reaction (24.6 mmol 1,2BDO/g_{Ir}.h, 28.2 mmol 2,3BDO/g_{Ir}.h, 4.2 mmol 1,4BDO/g_{Ir}.h and 3 mmol 1,4BDO/g_{Ir}.h).

Mechanism of BDO formation via C-O hydrogenolysis on $Ir/ReO_x/TiO_2$

Studies of hydrogenolysis of polyols, mainly glycerol, on $Ir/ReO_x/SiO_2$[72] and $Rh/ReO_x/TiO_2$[39] catalysts have reported a synergetic effect of Ir or Rh and ReO_x clusters suggesting that hydrogen is activated on Ir metal and then attacks the alkoxide formed by polyol adsorbed on ReO_x clusters. Thus, erythritol could be adsorbed on the surface of the ReO_x clusters at the terminal position or through a secondary OH group as previously discussed on other polyols molecules such as glycerol[72] and propanediols[44] and its further interaction with the H_2 activated on a close Ir atom determines which BTO isomer would be formed. A simple C-O hydrogenolysis of either 1,2,3BTO or 1,2,4BTO would produce BDO although some BDO isomers would also form directly from ERY. Indeed, 2,3BDO, the main product formed on $Ir/ReO_x/TiO_2$, could proceed from the rapidly transformation of 1,2,3BTO highly favored on this catalysts or from a double C-O hydrogenolysis of ERY as it was previously proposed on bimetallic/support catalyst[39] and in good agreement with the non-zero initial slope of 2,3BDO concentration curve as a function of time (Figure 8 E). Similarly, 1,2BDO, that was the second most abundant BDO isomer on $Ir/ReO_x/TiO_2$, could be formed by a C-O hydrogenolysis of either 1,2,3BTO or 1,2,4BTO and directly from ERY by a double C-O hydrogenolysis similarly to 2,3BDO formation or via hydrodeoxygenation. The reaction mechanism of hydrodeoxygenation (which implicates a deoxydehydration and further hydrogenation in only one step) would involve the coordination of vicinal OH groups of ERY to active Re^{+IV} species[73] as diolate; a further hydrogenation catalyzed by Ir would form 1,2BDO, although in aqueous phase on bimetallic Ir/ReO_x/support catalysts it would take place at low rate under the reaction conditions used. Finally, the C-O hydrogenolysis of 1,2,4BTO adsorbed through a primary or secondary OH group would render 1,4BDO and 1,3BDO respectively. Scheme 5 shows both the simple and double C-O hydrogenolysis routes specially for 1,2BDO formation even though they can be adapted for the other BDO isomers. All the C-O hydrogenolysis reactions proposed here on $Ir/ReO_x/TiO_2$ involve an H_2 molecule activated on Ir metallic sites together with ERY adsorbed on

partially reduced Re species to form the corresponding alkoxide. In this sense, the role of the redox support, especially when using TiO_2, would be to prevent the overreduction of Re species by the interaction between Re species and the TiO_2 surface favoring therefore the appropriate adsorption of ERY and the further C-O hydrogenolysis.

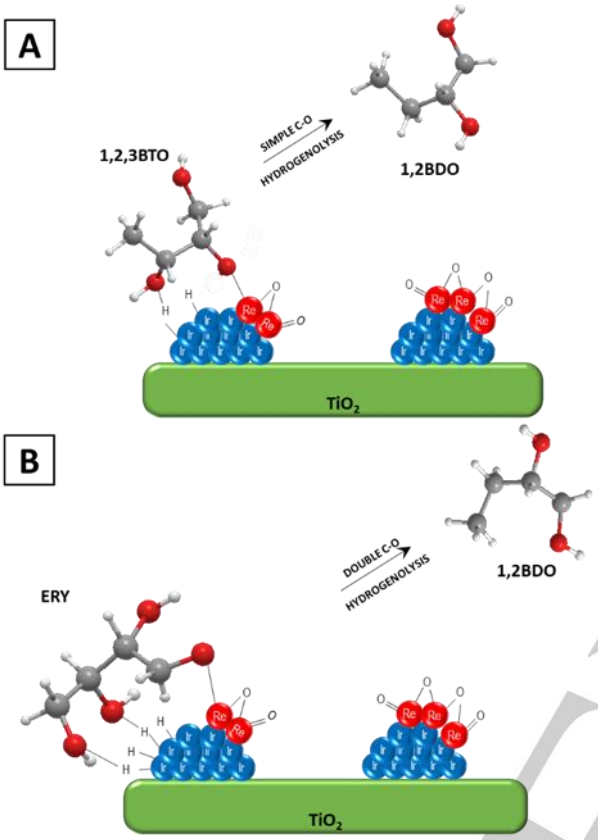

Scheme 5. Proposed pathways for 1,2BDO formation on $Ir/ReO_x/TiO_2$. (A) Simple C-O Hydrogenolysis and (B) Double C-O Hydrogenolysis.

Spent catalyst characterization

$Ir/ReO_x/TiO_2$ catalyst used during 30 h erythritol reaction was recovered by filtration, thoroughly washed with deionized water, dried at 373 K overnight (spent catalyst) and characterized by temperature programmed oxidation (TPO), ICP analysis, TEM, DRX and Raman. Experimental details about characterization of spent and spent-reduced (treated in H_2 flow at the same temperature than fresh sample) catalysts and their comparison with fresh $Ir/ReO_x/TiO_2$ is informed in Section S.7, Supporting Information.

The TPO profile for spent $Ir/ReO_x/TiO_2$ (Figure S7, Supporting Information) displayed two main peaks assigned to two different type of coke on catalyst surface. The amount of coke, determined by deconvolution and integration of TPO profile, was 1.6% C, i.e. 1.6 g of C per 100 g of catalyst.

Spent and spent-reduced samples were further characterized by X-ray diffraction and Raman spectroscopy. Both fresh and spent XRD diffractograms, displayed in in Figure S8, Supporting Information, are identical. DRX diffractograms show that the peaks attributed to anatase (~85%) and rutile (~15%) remain invariant when comparing fresh and spent catalysts. The peaks corresponding to Ir or Re oxides, 28° (IrO_2), 24.3° (ReO_2), 29.1° (ReO_3) and 24.6° (Re_2O_7), were not observed.

The Raman spectra for fresh, spent and spent-reduced $Ir/ReO_x/TiO_2$ samples for the 100–1200 cm^{-1} region are shown in Figures S9 and S10 of Supporting Information. The bands attributed to anatase were clearly detected in concordance with DRX results indicating that anatase is the main phase of TiO_2. It was previously reported that the spectrum of Ir/SiO_2 displayed two peaks at 708 and 548 cm^{-1} attributed to the IrO_2 phase[74]. None of these peaks were detected in the fresh and spent-reduced $Ir/ReO_x/TiO_2$ spectra and only a very small peak at about 705 cm^{-1} and a shoulder at 544 cm^{-1} were observed for spent $Ir/ReO_x/TiO_2$. This finding corroborates that Ir oxide is not formed on both fresh and spent-reduced catalysts but probably small amounts of IrO_2 are present on spent catalyst before treatment with H_2 flow. The spectrum for fresh $Ir/ReO_x/TiO_2$ displayed a small band at about 980 cm^{-1} due to Re species with partially oxidized Re[75] that remained almost identical in spent and spent-reduced catalysts; in addition a very small band at 1040 cm^{-1} was observed for spent catalyst probably suggesting a slight modification of some Re oxides species. Nevertheless, there are no structural differences in Re species between fresh and spent-reduced $Ir/ReO_x/TiO_2$ according to Raman and DRX results. Finally, no bands in the Raman region between 1100 and 1800 cm^{-1}, which corresponds to the coke bands, were detected in the spent or spent-reduced catalysts (Figure S11, Supporting Information) in good agreement with the very low coke content according to TPO results.

Spent-reduced Ir/ReOx/TiO2 sample was also characterized by transmission electron microscopy; a representative TEM image and the size distribution histogram are shown in Figure 9. The mean particle size was 1.75 nm which is very similar to that for the fresh catalyst.

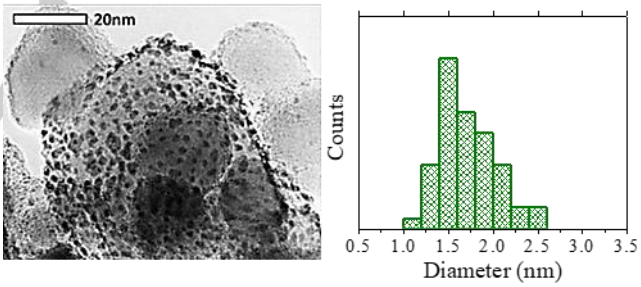

Figure 9. Representative TEM image and size distribution associated with $Ir/ReO_x/TiO_2$ spent-reduced catalyst.

Catalyst reusability

Two consecutive reactions were conducted to study the catalyst reusability. Thus, $Ir/ReO_x/TiO_2$ catalyst used during 30 h erythritol reaction was recovered, thoroughly washed with deionized water, dried at 373 K overnight and reduced at the same temperature than fresh catalyst. The spent-reduced $Ir/ReO_x/TiO_2$ sample was tested in a second 30 h reaction cycle under the same reaction conditions and results are informed in Figure 9. The ERY conversion curve as a function of time was very similar during both reactions while the liquid products distribution was slightly different. Thus, the BTO concentration increased whereas both the BDO and BuOH concentrations decreased; the concentration of products from C-C hydrogenolysis and threitol increased while the formation of

dehydration products decreased. These results suggest that small changes on catalyst surface took place even when characterization of spent-reduced catalyst are almost identical than the fresh one.

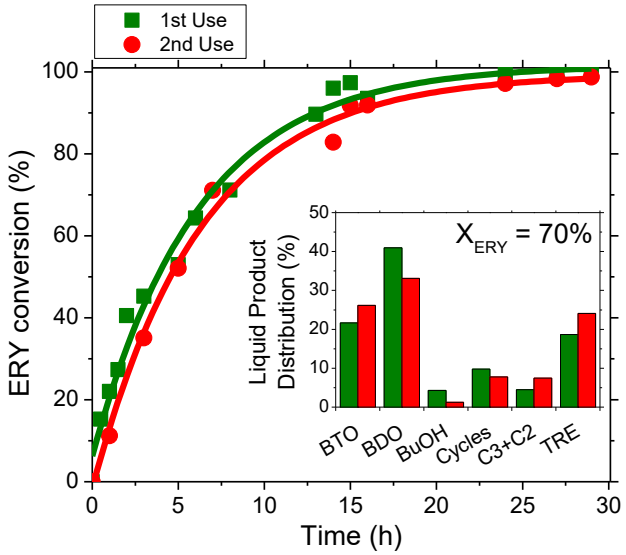

Figure 10. Catalytic results after $Ir/ReO_x/TiO_2$ re-use [473K, P_{H2}=25bar, C^0_{ERY}=0.4 M, C_{cat}=0.0125 g/cm^3].

Conclusion

The hydrogenolysis of an aqueous solution of erythritol on Ir/ReO_x supported (2 wt. % Ir, Re/Ir molar ratio ≈ 1) on solids of different nature was studied. All the catalysts were thoroughly characterized using several techniques (such as N_2 physisorption, NH_3 TPD, TPR, TEM microscopy, CO chemisorption and XPS) that allowed proposing different surface models for Ir and ReO_x species on each support. The physicochemical, redox and acidic properties of the supports notably influenced on the metal dispersion, reducibility of the species and particle sizes and consequently, the catalytic performance was also affected. It was demonstrated that the acidity of the support catalyzes dehydration reactions and therefore, high concentration of 1,4AE was achieved on Ir/ReO_x supported on Al_2O_3, AC and ZrO_2. $Ir/ReO_x/TiO_2$ selectively promoted the C-O hydrogenolysis over the other competitive pathways including C-C scissions and dehydrations and a maximum yield to butanediols of 53 % at 24 h of reaction was reached. Actually, XPS, TPR and CO chemisorption results allowed explaining the catalytic results by determining that the small particle size, the accessibility to the metallic Ir atoms and the intimate contact between Ir and ReO_x species, with Re mainly as Re^{+IV}, on $Ir/ReO_x/TiO_2$ selectively promoted the C-O hydrogenolysis pathways. Thus, the role of the redox support, especially when using TiO_2, would be to prevent the overreduction of Re species by the interaction between ReO_x and the TiO_2 surface favoring therefore the adsorption of ERY on ReO_x species in close contact to metallic Ir and the further C-O scission.

1,2BDO was the predominant BDO isomer formed except on $Ir/ReO_x/TiO_2$ that favored the 2,3BDO formation followed by 1,2 BDO and 1,3BDO; 1,4BDO concentrations were low on all the catalysts. Catalytic results using $Ir/ReO_x/TiO_2$ suggested that 2,3BDO can be formed by the rapidly C-O hydrogenolysis of the primary product 1,2,3BTO highly favored on this catalyst or directly from ERY by a double C-O hydrogenolysis. Instead, 1,2BDO can be produced by C-O scissions of both 1,2,3BTO and 1,2,4BTO and also directly from reactant either by double C-O hydrogenolysis (similarly to 2,3BDO) or, in less extent, by hydrodeoxygenation. 1,3BDO and 1,4BDO were formed by two successive C-O hydrogenolysis with butanetriols as intermediate compounds. In addition, some contribution to 1,2BDO, 1,3BDO and 2,3BDO formation from 1,4AE may take place on catalysts supported on Al_2O_3, AC and ZrO_2 that significantly formed this dehydration product from ERY.

Overall, $Ir/ReO_x/TiO_2$ allowed obtaining a maximum BDO productivity of 60 mmol/g_{Ir}.h (24.6 mmol 1,2BDO/g_{Ir}.h, 28.2 mmol 2,3BDO/g_{Ir}.h, 4.2 mmol 1,4BDO/g_{Ir}.h and 3 mmol 1,4BDO/g_{Ir}.h), which is three times higher than the values reported for traditionally SiO_2 based bimetallic catalysts because of the combination of appropriate noble metal (Ir), oxophilic promoter (Re) and a support with reduced surface area and redox characteristic like TiO_2. Finally, $Ir/ReO_x/TiO_2$ can be re-used preserving its original activity.

Experimental Section

Catalysts preparation

Six solids with different acidic and textural properties were employed as support of Ir/ReO_x catalysts: CeO_2 prepared in our laboratory and commercial supports such as SiO_2 (Sigma Aldrich Grade 62), Al_2O_3 (CK-300), ZrO_2 (Daiichi Kigenso RC-100), TiO_2 (Evonik P25) and activated carbon (AC, Degussa). CeO_2 was synthesized by precipitation according to methods previously reported[76]. An aqueous solution of NH_4OH (28%) was added dropwise to a 0.7 M solution of $Ce(NO_3)_3.6H_20$ (Aldrich) in a stirred batch reactor at 333 K until pH=9. The precipitate was maintained at pH=9 and aged for 1 h at 333 K. The solid was filtered, washed thoroughly with deionized water at 333 K, dried at 373 K overnight and treated in air flow at 673 K for 4 h. Ir/ReO_x catalysts were prepared by consecutive incipient wetness impregnation technique. Prior to impregnation, the supports were treated 2 h in air flow (48 cm^3/min. $g_{catalyst}$) at 723 K, except the AC, whose thermal treatment was carried out in flowing N_2. Successive impregnations were conducted by first incorporating the Ir using an aqueous solution of H_2IrCl_6 (Sigma, 99.98%), and then Re from a solution of NH_4ReO_4 (Sigma Aldrich, 99%); these solids were dried at 373 K for 12 h after each impregnation. Finally, the prepared catalysts were treated in the same way as the supports in air or N_2 flow.

Catalysts characterization

The surface areas (S_{BET}) were determined by physisorption of N_2 at 77 K in a Micromeritics Model ASAP 2020 sorptometer. Prior to N_2 physisorption, samples were degassed for 3 h at 573 K. The structure of the supports and catalysts were corroborated by XRD using a X-ray diffractometer XD-D1 with monochromatic Cu radiation Kα filtered with Ni. The metal content (Ir and Re) of the catalysts was determined by inductively coupled plasma atomic emission spectroscopy ICP-AES (Perkin Elmer, Optima 2100 DV).

Catalysts acidity was studied by temperature programmed desorption (TPD) of NH_3 preadsorbed at 373 K as described elsewhere[77]. Samples (0.1 g) were treated in flowing He (60 cm^3/min) at 723 K for 2 h and then exposed to a 1% NH_3/He stream for 40 min at 373 K. Weakly adsorbed

NH_3 was removed by flowing He at 373 K for 1 h; then the temperature was increased (10 K/min) and the NH_3 concentration in the effluent was measured by mass spectrometry in a Baltzers Omnistar unit.

The reducibility of the catalysts was determined by reduction at programmed temperature (TPR) in a flow equipment coupled to a mass spectrometer Baltzers Omnistar unit using 60 cm^3/min of 5% H_2/Ar and a heating rate of 10 K/min from 298 to 1023 K. The reduction temperature of the first peak of TPR profiles was selected to ensure that Ir was found as Ir^0 and Re as partially reduced species. Thus, these temperatures were used to pretreatments before reaction or characterization techniques such as XPS and TEM measurements.

The Ir dispersion (D_{CO}) of the catalysts was determined by CO chemisorption, using the double isotherm method in a volumetric adsorption experiment, and considering that CO is not adsorbed on rhenium oxides[39]. Catalysts (0.1-0.5 g) were reduced using H_2 at specific temperature for 1 h before adsorption measurements and then evacuated (1.3 10^{-5} mbar) at the same temperature during 1 h. The CO adsorption was carried out at room temperature and the first isotherm was obtained accounting for the total CO uptake. Subsequently, the sample was evacuated for 15 min at room temperature and a second isotherm was conducted to determine the amount of weakly adsorbed CO. From the subtraction of the two isotherms, the quantity of strongly bound CO was determined.

Transmission electron microscope (TEM) images were acquired with JEOL 2100 plus instrument. The samples were dispersed in ethanol using ultrasound and supported on Cu grids. More than 200 particles were measured to estimate the particle size distribution and average particle size (d_{pTEM}) defined as: $d_{pTEM} = \frac{\sum n_i . d_i^3}{\sum n_i . d_i^2}$ where n_i is the number of particles with d_i diameter.

XPS analysis was performed on a Specs Multitechnical instrument equipped with a dual Al/Mg X-ray source and a PHOIBOS 150 hemispheric analyzer in fixed analyzer transmission mode (FAT). The spectra were obtained with step energy of 30 eV with an anode of Mg operated at 200 W. The pressure during the measurement was less than 1.10^{-9} mbar. The samples were supported on sample holders of the instrument and treated in 5% H_2/Ar flow during 30 minutes at the temperature determined from TPR experiments, and then evacuated in ultra-high vacuum for 2 h before reading.

Catalytic tests

Catalytic tests were carried out in a batch reactor (Parr 4565). Catalysts were previously reduced ex-situ in H_2 flow (50 cm^3/min. $g_{catalyst}$) at the reduction temperature of the Ir, determined by TPR, and then transferred to the reactor. Prior reaction, the catalyst was subjected to a second reduction inside the reactor following a previously reported procedure[41]. In standard conditions, 34 cm^3 of deionized water and 0.5 g of catalyst were added into the reactor (catalyst concentration = C_{cat} = 0.0125 g/cm^3) and the air was eliminated by purged with N_2. Afterwards, the reactor was pressurized with H_2, heated to the set temperature and remained at this value for 1 h to conduct the *in situ* reduction. Then, the reactor was cooled at 363 K and an ERY solution (calculated for reaching an ERY concentration of 0.4 M inside the reactor) was introduced together with 1.5 µL of H_2SO_4 (Sigma, 96%). The total volume of liquid inside the reactor was 40 cm^3. It was reported[41,72] that the addition of this small amount of H_2SO_4 prevents the Ir and Re leaching in the reaction media. Once the reaction temperature has been reached, 25 bar of H_2 are added, considering this moment as the initial time. The analysis of the liquid phase was carried out in a Shimadzu 20A HPLC Chromatograph with IR detector (RID-20A), using a Bio-Rad Aminex HPX-87H column at 328 K, with a flow rate of mobile phase (H_2SO_4 5mM) of 0.6 cm^3/min.
The erythritol conversion (X_{ERY}) was calculated as:

$$X_{ERY}(\%) = \frac{C_{ERY}^0 - C_{ERY}^t}{C_{ERY}^0} \cdot 100 \quad (1)$$

where C_{ERY}^0 is the initial ERY concentration in the reactor and C_{ERY}^t is the ERY concentration at a time *t* of reaction.

The yield to *j* product (η_j^t):

$$\eta_j^t = \frac{C_j^t \cdot n_j}{C_{ERY}^0 \cdot n_{ERY}} \cdot 100 \quad (2)$$

where C_j^t is the *j* product concentration at a time *t* of reaction, n_j is number of carbon atoms in *j* product and n_{ERY} is number of carbon atoms in ERY (n_{ERY}=4).

The carbon mass balance (CB^t) was calculated considering erythritol and all the products as:

$$CB^t = \frac{total\ carbon\ atoms\ at\ t\ time}{total\ carbon\ atoms\ at\ t=0} = \frac{\sum_{j=1}^{n} C_j^t \cdot n_j + C_{ERY}^t \cdot n_{ERY}}{C_{ERY}^0 \cdot n_{ERY}} \quad (3)$$

Acknowledgements

Financial support of Universidad Nacional del Litoral (UNL), Consejo Nacional de Investigaciones Científicas y Técnicas (CONICET), and Agencia Nacional de Promoción Científica y Tecnológica (ANPCyT), Argentina is gratefully acknowledged as well as ANPCyT for the purchase of the SPECS multitechnique analysis instrument (PME8-2003).

Keywords: butanediols • erythritol • hydrogenolysis • Ir catalysts • Re catalysts

References

[1] A. Corma, S. Iborra, A. Velty, *Chem. Rev.* **2007**, *107*, 2411–2502.
[2] R. M. West, E. L. Kunkes, D. A. Simonetti, J. A. Dumesic, *Catal. Today* **2009**, *147*, 115–125.
[3] J. J. Bravo-Suárez, R. V. Chaudhari, B. Subramaniam, *ACS Symp. Ser.*, **2013**, pp. 3–68.
[4] H.-J. Moon, M. Jeya, I.-W. Kim, J.-K. Lee, *Appl. Microbiol. Biotechnol.* **2010**, *86*, 1017–1025.
[5] Y. Ryu, C. Y. Park, J. B. Park, S. Y. Kim, J.-H. Seo, *J. Ind. Microbiol. Biotechnol.* **2000**, *25*, 100–103.
[6] H. Ishizuka, K. Wako, T. Kasumi, T. Sasaki, *J. Ferment. Bioeng.* **1989**, *68*, 310–314.
[7] Y. Nakagawa, T. Kasumi, J. Ogihara, M. Tamura, T. Arai, K. Tomishige, *ACS Omega* **2020**, *5*, 2520–2530.
[8] M. A. Y. Aoki, G. M. Pastore, Y. K. Park, *Biotechnol. Lett.* **1993**, *15*, 383–388.
[9] M. Hiele, Y. Ghoos, P. Rutgeerts, G. Vantrappen, *Br. J. Nutr.* **1993**, *69*, 169–176.
[10] R. Mizanur, K. Takeshita, H. Moshino, G. Takada, K. Izumori, *J. Biosci. Bioeng.* **2001**, *92*, 237–241.
[11] X. Ji, H. Huang, P. Ouyang, *Biotechnol. Adv.* **2011**, *29*, 351–364.
[12] D. G. Barrett, W. Luo, M. N. Yousaf, *Polym. Chem.* **2010**, *1*, 296–302.
[13] E. Arceo, J. A. Ellman, R. G. Bergman, *J. Am. Chem. Soc.* **2010**,

132, 11408–11409.
[14] M. Shiramizu, F. D. Toste, *Angew. Chemie - Int. Ed.* **2012**, *51*, 1–6.
[15] M. W. Marshall Tuck, M. A. Wood, A. G. Hiles, *Process for the Production of 1,4- Butanediol, y-Butyrolactone and Tetrehydrofuran*, **1997**, 6100410.
[16] T. Haas, B. Jaeger, R. Weber, S. F. Mitchell, C. F. King, *Appl. Catal. A Gen.* **2005**, *280*, 83–88.
[17] A. Burgard, M. Burk, R. Osterhout, J. Sun, P. Pharkya, *Microorganisms for Producing 1,3-Butanediol and Methods Related Thereto*, **2018**, 9982281.
[18] R. Hasegawa, K. Hayashi, F. Application, P. Data, P. E. Trousof, *Polyester Containing Impure 1,2-Butanediol*, **1986**.
[19] C. Liang, Z. Ma, L. Ding, *Catal. Letters* **2009**, *130*, 169–176.
[20] O. M. Daniel, A. Delariva, E. L. Kunkes, A. K. Datye, J. A. Dumesic, R. J. Davis, *ChemCatChem* **2014**, *2*, 1107–1114.
[21] Y. Nakagawa, X. Ning, Y. Amada, K. Tomishige, *Appl. Catal. A Gen.* **2012**, *434*, 128–134.
[22] L. Liu, T. Asano, Y. Nakagawa, M. Tamura, K. Okumura, K. Tomishige, *ACS Catal.* **2019**, *9*, 10913–10930.
[23] C. Montassier, D. Giraud, J. Barbier, *Polyol Conversion by Liquid Phase Heterogeneous Catalysis Over Metals*, **1988**.
[24] E. P. Maris, R. J. Davis, *J. Catal.* **2007**, *249*, 328–337.
[25] K. Tomishige, Y. Nakagawa, M. Tamura, *Curr. Opin. Green Sustain. Chem.* **2020**, *22*, 13–21.
[26] C. Montassier, J. C. Mcnczo, L. C. Hoang, C. Renaud, J. Barbier, *J. Mol. Catal. A Chem.* **1991**, *70*, 99–110.
[27] D. G. Lahr, B. H. Shanks, *J. Catal.* **2005**, *232*, 386–394.
[28] I. M. Leo, M. L. Granados, J. L. G. Fierro, R. Mariscal, *Chinese J. Catal.* **2014**, *35*, 614–621.
[29] P. J. C. Hausoul, A. K. Beine, L. Neghadar, R. Palkovits, *Catal. Sci. Technol.* **2017**, *7*, 56–63.
[30] T. Miyazawa, Y. Kusunoki, K. Kunimori, K. Tomishige, *J. Catal.* **2006**, *240*, 213–221.
[31] W. Zhou, Y. Zhao, S. Wang, X. Ma, *Catal. Today* **2017**, *298*, 2–8.
[32] M. Checa, A. Marinas, J. M. Marinas, F. J. Urbano, *Appl. Catal. A Gen.* **2015**, *507*, 34–43.
[33] Y. Shinmi, S. Koso, T. Kubota, Y. Nakagawa, K. Tomishige, *Appl. Catal. B Environ.* **2010**, *94*, 318–326.
[34] V. Montes, M. Checa, A. Marinas, M. Boutonnet, J. M. Marinas, *Catal. Today* **2014**, *223*, 129–137.
[35] L. Ma, D. He, *Catal. Today* **2010**, *149*, 148–156.
[36] Z. Wang, B. Pholjaroen, M. Li, W. Dong, N. Li, A. Wang, X. Wang, Y. Cong, T. Zhang, *J. Energy Chem.* **2014**, *23*, 427–434.
[37] M. Chia, Y. J. Pagán-Torres, D. Hibbitts, Q. Tan, H. N. Pham, A. K. Datye, M. Neurock, R. J. Davis, J. A. Dumesic, *J. Am. Chem. Soc.* **2011**, *133*, 12675–12689.
[38] K. Chen, S. Koso, T. Kubota, Y. Nakagawa, *ChemCatChem* **2010**, *2*, 547–555.
[39] A. Said, D. Da Silva Perez, N. Perret, C. Pinel, M. Besson, *ChemCatChem* **2017**, *9*, 2768–2783.
[40] M. Gu, L. Liu, Y. Nakagawa, C. Li, M. Tamura, Z. Shen, X. Zhou, Y. Zhang, K. Tomishige, *ChemSusChem* **2021**, *14*, 489.
[41] Y. Amada, H. Watanabe, Y. Hirai, Y. Kajikawa, Y. Nakagawa, K. Tomishige, *ChemSusChem* **2012**, *5*, 1991–1999.
[42] A. Said, D. Da Silva Perez, N. Perret, C. Pinel, M. Besson, *ChemCatChem* **2017**, *9*, 2768–2783.
[43] Y. Amada, Y. Shinmi, S. Koso, T. Kubota, Y. Nakagawa, K. Tomishige, *Appl. Catal. B Environ.* **2011**, *105*, 117–127.
[44] Y. Amada, S. Koso, Y. Nakagawa, K. Tomishige, *ChemSusChem* **2010**, *3*, 728–736.
[45] A. B. Dongil, C. Rivera-Carcamo, L. Pastor-Perez, A. Sepulvado-Escribano, P. Reyes, *Catal. Today* **2014**, *249*, 72–78.
[46] A. Ciftci, D. A. J. M. Ligthart, A. O. Sen, A. J. F. Van Hoof, H. Friedrich, E. J. M. Hensen, *J. Catal.* **2014**, *311*, 88–101.
[47] B. J. Kip, J. Van Grondelle, J. H. A. Martens, R. Prins, *Appl. Catal.* **1986**, *26*, 353–373.
[48] Y. Huang, A. Wang, X. Wang, T. Zhang, *Int. J. Hydrogen Energy* **2007**, *32*, 3880–3886.
[49] A. Trovarelli, *Catal. Rev.* **2006**, *38*, 439–520.
[50] O. Hernandez-Cristobal, G. Diaz, A. Gomez-Cortes, *Ind. Eng. Chem. Res.* **2014**, *53*, 10097–10104.
[51] M. A. Vuurman, D. J. Stufkens, A. Oskam, I. E. Wachs, *J. Mol. Catal.* **1992**, *76*, 263–285.
[52] P. Arnoldy, E. M. van Oers, O. S. Bruinsma, V. H. de Beer, J. A. Moulijn, *J. Catal.* **1985**, *93*, 231–245.
[53] Y. Amada, N. Ota, M. Tamura, Y. Nakagawa, **2014**.
[54] M. Chia, Y. J. Pag, D. Hibbitts, Q. Tan, H. N. Pham, A. K. Datye, M. Neurock, R. J. Davis, J. A. Dumesic, *J. Am. Chem. Soc.* **2011**, *133*, 12675–12689.
[55] E. M. Virgilio, C. Padró, M. E. Sad, *Lat. Am. Appl. Res.* **2020**, *50*, 89–94.
[56] Y. Amada, H. Watanabe, M. Tamura, Y. Nakagawa, K. Okumura, K. Tomishige, *J. Phys. Chem. C* **2012**, *116*, 23503–23514.
[57] J. F. Moulder, W. F. Stickle, P. E. Sobol, K. D. Bomben, *Handbook of X-Ray Photoelectron Spectroscopy*, **1992**.
[58] M. Cohen Sagiv, N. Eliaz, E. Gileadi, *Electrochim. Acta* **2013**, *88*, 240–250.
[59] W. T. Tysoe, F. Zaera, G. A. Somorjai, *Surf. Sci.* **1988**, *200*, 1–14.
[60] S. Koso, Y. Nakagawa, K. Tomishige, *J. Catal.* **2011**, *280*, 221–229.
[61] N. Ota, M. Tamura, Y. Nakagawa, K. Okumura, *Angew. Chem., Int. Ed.* **2014**, *53*, 1–5.
[62] K. Tomishige, M. Tamura, Y. Nakagawa, *Chem. Rec.* **2014**, *14*, 1041–1054.
[63] S. Koso, H. Watanabe, K. Okumura, Y. Nakagawa, K. Tomishige, *J. Phys. Chem.* **2012**, *116*, 3079–3090.
[64] S. Koso, H. Watanabe, K. Okumura, Y. Nakagawa, K. Tomishige, *Appl. Catal. B Environ.* **2012**, *112*, 27–37.
[65] N. Ota, M. Tamura, Y. Nakagawa, K. Okumura, K. Tomishige, *ACS Catal.* **2016**, *6*, 3213–3226.
[66] L. Liu, T. Asano, Y. Nakagawa, M. Tamura, K. Tomishige, *Green Chem.* **2020**, *22*, 2375–2380.
[67] G. Hudson, R. Barker, *J. Org. Chem.* **1967**, *32*, 3650–3658.
[68] X. Xiaoding, J. C. Mol, C. Boelhouwer, *J. Am. Chem. Soc.* **1986**, *82*, 2707–2718.
[69] A. Ciftci, D. A. J. M. Ligthart, A. O. Sen, A. J. F. Van Hoof, H. Friedrich, E. J. M. Hensen, *J. Catal.* **2014**, *311*, 88–101.
[70] T. Miyazawa, S. Koso, K. Kunimori, K. Tomishige, *Appl. Catal. A Gen.* **2007**, *318*, 244–251.
[71] E. S. Vasiliadou, T. M. Eggenhuisen, P. Munnik, P. E. De Jongh, K. P. De Jong, A. A. Lemonidou, *Appl. Catal. B Environ.* **2014**, *145*, 108–119.
[72] Y. Nakagawa, Y. Shinmi, S. Koso, K. Tomishige, *J. Catal.* **2010**, *272*, 191–194.
[73] N. Ota, M. Tamura, Y. Nakagawa, K. Okumura, K. Tomishige, *ACS*

Catal. **2016**, *6*, 3213–3226.

[74] Y. Amada, H. Watanabe, M. Tamura, Y. Nakagawa, K. Okumura, K. Tomishige, *J. Phys. Chemi* **2012**, *116*, 23503–23514.

[75] J. Mol, *Catal. Today* **1999**, *51*, 289–299.

[76] S. Rossignol, Y. Madier, D. Duprez, *Catal. Sci. Technol.* **1999**, *50*, 261–270.

[77] C. Padro, M. E. Sad, C. Apesteguia, *Catal. Today* **2006**, *116*, 184–190.

Entry for the Table of Contents

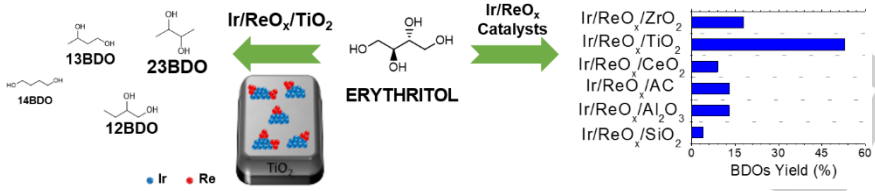

$Ir/ReO_x/TiO_2$ favors C-O hydrogenolysis and minimizes C-C scissions and dehydration reactions due to the intimate contact between Ir and ReO_x on this support (small particle size) and the presence of Ir mostly in metallic state and partially oxidized Re species (mainly Re^{+IV}).